[redacted]

# AD 350496L

## DEFENSE DOCUMENTATION CENTER

FOR

## SCIENTIFIC AND TECHNICAL INFORMATION

CAMERON STATION, ALEXANDRIA, VIRGINIA

[redacted]

[redacted]

NWL Report No. 1821

NAVWEPS REPORT NO. 7673

Copy No. 25





# PRELIMINARY
# WARHEAD TERMINAL BALLISTIC HANDBOOK
## Part I
## Terminal Ballistic Effects (U)

by

C. Johnson and J. W. Moseley

Warhead and Terminal Ballistics Laboratory

U. S. NAVAL WEAPONS LABORATORY

DAHLGREN, VIRGINIA





[redacted]

[redacted]

U. S. Naval Weapons Laboratory
Dahlgren, Virginia

PRELIMINARY
WARHEAD TERMINAL BALLISTIC HANDBOOK

Part I - Terminal Ballistic Effects (U)

by

C. Johnson and J. W. Moseley
Warhead and Terminal Ballistics Laboratory

NWL Report No. 1821
NAVWEPS Report No. 7673

31 MAR 1964



[redacted]

## TABLE OF CONTENTS - PART I





[redacted]

TABLE OF CONTENTS - PART I (Continued)





[redacted]

TABLE OF CONTENTS - PART I (Continued)

TABLE OF CONTENTS - PART I (Continued)

## TABLE OF CONTENTS - PART I (Continued)

## TABLE OF CONTENTS - PART I (Conti[redacted]



TABLES - PART I



 [redacted]

[redacted]

ABSTRACT

This report is contained in two separate parts.

Part I, Terminal Ballistic Effects, presents a summary of the laws, parameters and equations associated with conventional kill mechanisms.

Part II, Warhead Terminal Ballistic Performance, presents specific MARK warhead descriptions and basic data on warhead terminal ballistic performance for approximately forty-seven Guided Missile Warheads, Bombs, Rocket Warheads, and Projectiles.

[redacted]

## FOREWORD

The Bureau of Naval Weapons assigned to the Naval Weapons Laboratory, by BUWEPS WEPTASK RMMO-42-003/210-1/F008-08-006, a task with the objectives of (1) establishing and maintaining a handbook of terminal ballistic performance data for all current nonnuclear ordnance, (2) developing and defining generalized lethality criteria suitable for the specification or determination of warhead terminal ballistic performance, and (3) improving projectiles and rocket warheads, utilizing current developments in warhead technology.

This is the first formal report on the assigned task and is limited to objective (1) discussed above. The report is contained in two separate parts. Part I, Terminal Ballistic Effects, presents a summary of the laws, parameters and equations associated with conventional kill mechanisms. Part II, Warhead Terminal Ballistic Performance, presents a description of specific MARK warheads and includes all available data collected and analyzed by the time of publication. Additional data and discussions not included in this preliminary publication are scheduled for inclusion by future revision or publication. The ultimate aim of this publication is to provide data on warhead terminal ballistic performance in a form and quantity which will be immediately useful in preparing directives or guides for conventional weapons selection and in conducting weapon effectiveness studies.

This report has been reviewed by the following personnel of the Warhead and Terminal Ballistics Laboratory:

C. A. COOPER, Acting Chief, Project Engineering Branch
W. W. MEYERS, Head, Development Division
W. G. SOPER, Assistant for Theory and Analysis
W. E. McKENZIE, Assistant Director for Technical Applications
R. I. ROSSBACHER, Director

APPROVED FOR RELEASE:

/s/ RALPH A. NIEMANN
Acting
Technical Director



[redacted]

## INTRODUCTION - PART I

This part of the Preliminary Handbook of Warhead Terminal Ballistic Performance contains summary discussions of conventional kill mechanisms. These summaries include discussions of the basic laws and parameters associated with the kill mechanisms.

The discussions included in this edition of the handbook are presented in four sections:

Section 1 - Fragmentation

Section 2 - Blast

Section 3 - Penetration

Section 4 - Shaped Charges

Section 1, Fragmentation, provides discussions of the theories concerned with the natural fragmentation of conventional warheads and presents experimental data for determining the values of the constants utilized in the theoretical discussions.

Section 2, Blast, is scheduled to include discussions concerning Blast-External, Blast-Internal, Earth Shock, Cratering, and Blast Measurements. However, this preliminary edition only presents a review of the theories and experimental data concerned with the effects that such parameters as charge composition, charge geometry, casing material, atmospheric pressure and temperature and mach wave reflections have on <u>external blast</u>.

Section 3, Penetration, presents discussions of some of the various empirical formulae dealing with the penetration of armor by projectiles. A brief discussion of the perforation of mild steel by fragments is also presented.

Discussions of the penetration of concrete and soil by projectiles are scheduled to be included in the next edition of the handbook.

Section 4, Shaped Charges, is presented to familiarize the reader with the principles of the shaped charge. Theories, theoretical formulae and empirical formulae pertaining to cone collapse, jet formation, and jet penetration are included as well as brief discussions of factors affecting penetration. These factors are included under such topics as liner shape, standoff distance, explosive preparation, and warhead casing design. Scheduled for the next edition are discussions on such topics as effects of rotation upon jets, vaporific effects, damage mechanisms, fuze action, perforation damage, spin compensation, and defeat of shaped charge weapons.

# SECTION I
# FRAGMENTATION

## 1.1 INTRODUCTION

The natural fragmentation characteristics of conventional warheads are usually placed in three general classes, fragment velocity, directional distribution, and mass distribution. Fragment velocity varies with distance of travel and each of the characteristics are affected by such parameters as explosive composition, type and thickness of casing material, and the warhead geometry in general.

The purpose of this section is to provide a brief discussion of the theories concerned with the above characteristics, and to present experimental data for determining the values of the constants utilized in the theoretical discussion.

Methods are available for designing warheads that will produce fragments of a predetermined size (controlled fragmentation); however, since the use of controlled fragmenting warheads is generally limited to attack of specific targets which are primarily vulnerable to fragments of an optimum size these methods are not widely employed among the warheads documented in Part II. For this reason only a brief discussion of some of the more important methods of controlling fragment size is presented.

1.1.1 FRAGMENTATION PROCESS - GENERAL. Conventional fragmentation warheads consist of a high explosive (HE) charge, fuze and booster all enclosed in a metal casing. Upon detonation of the HE charge, the metal casing expands very rapidly, usually to about 1-1/2 times its original diameter[1-1], and then breaks into fragments. The rate of expansion depends on the composition and weight of the explosive filler, type and thickness of casing material, and the geometric configuration of the warhead in general. When the casing breaks up, the resulting fragments fly off, usually in a direction perpendicular to the surface of the expanded casing, at the same speed that the casing had attained during its expansion; little or no additional velocity increase occurs after the casing ruptures[1-2]. Within a very short distance from the center of explosion the fragments pass through the shock wave, which is retarded by the air to a greater extent than the fragments.

In effect, the high velocity fragments are projectiles with a potential capability of inflicting damage to adjacent objects. The potential damage capability depends upon such parameters as fragment mass, velocity, and distribution which are discussed in paragraph 1.2 below.

1.2 PARAMETERS INVOLVED IN THE FRAGMENTATION PROCESS

1.2.1 MASS DISTRIBUTION - MOTT[1-1]. The mass (m) and mass distribution of fragments from natural fragmenting warheads have been described theoretically in terms of simple exponential functions of m. The most widely used of these are the formulae introduced by Mott and Linfoot[1-3], which in general, apply fairly well to all modern fragmentation warheads.

1.2.1.1 Two-Dimensional Breakup. It was proposed in reference 1-3 that fragmentation of warheads which utilize thin-walled casings is the result of two-dimensional breakup. Under this assumption, along with the assumption that two-dimensional breakup holds down to the finest fragments, the mass distribution of the fragments may be approximated by the equation:

$$N(m) = N_o \, e^{-\left(\frac{m}{\mu}\right)^{1/2}} \tag{1-1}$$

where:

$N(m)$ = number of fragments of mass greater than (m)

$N_o$ = total number of fragments ($M/2\mu$)

$2\mu$ = arithmetic average fragmen mass

$M$ = total mass of warhead case (same units as $\mu$)

$e$ = base of natural logarithms

It should be noted that Mott's equation (1-1) assumes the warhead casing to be a cylinder. Although this is not generally true, satisfactory results can be obtained by considering the casing as a series of cylindrical segments and computing fragment mass distribution for each segment separately.

1.2.1.2 Three-Dimensional Breakup. It is postulated[1-4] that a large number of fragments, whose size is not influenced by casing thickness, may result from the fragmentation of an exceptionally thick-cased warhead. Under this condition the fragmentation process obeys the law of three-dimensional breakup, and the mass distribution of fragments will be described by

$$N(m) = N_o \, e^{-\left(\frac{m}{\mu}\right)^{1/3}} \qquad (1\text{-}2)$$

where:

$N(m)$ = number of fragments of mass greater than $(m)$

$N_o$ = total number of fragments $(M/6\mu)$

$6\mu$ = arithmetic average fragment mass

$M$ = total mass of warhead case

There is no set procedure for determining the exact casing thickness of warheads at which transition from two-dimensional breakup to three-dimensional breakup begins. However, it is stated in reference 1-4 that "most service projectiles having a wall thickness (before expansion) not greater than about 0.6 inch fall into the category of two-dimensional breakup".

1.2.1.3 Mott Scaling Formulae[1-5]. The value of the parameter $\mu$ is related to the inside diameter $(d_i)$ and thickness $(t)$ of the warhead casing by the empirical relation:

$$\mu^{1/2} = B \, t^{5/6} \, d_i^{\,1/3} \left(1 + \frac{t}{di}\right) \qquad (1\text{-}3)$$

where:

$\mu$ is in grams

B has the units of $gm^{1/2}$ $in.^{-7/6}$ and depends upon the explosive composition and the physical characteristics of the casing material

and

t and di are in inches

For small values of C/M, the charge-to-metal-mass ratio, equation (1-3) agrees very well with the formula proposed by Gurney and Sarmousakis (see paragraph 1.2.2) although in general these formulae do not agree. A comparison of these formulae with data obtained from two recent tests conducted at NWL, Dahlgren is shown on Figure 1-1. The comparison indicates that Mott's scaling formula more nearly represents the experimental data than does the Gurney-Sarmousakis formula.

The two test vehicles were cylinders loaded with H-6 explosive. The inside diameter, wall thickness, and length of each cylinder was 10.209 inches; .278 inch, and 15 inches respectively. One cylinder was fabricated from AISI-C1045 steel with a Rockwell hardness of approximately 98-B. The other cylinder was machined from the cylindrical section of a BULLPUP A warhead (AISI 4340 forged steel with a Rockwell hardness of approximately 36-C).

1.2.2 GURNEY-SARMOUSAKIS SCALING FORMULA. The relationship between $\mu$, the thickness (t), and inside diameter ($d_i$) of the casing will, according to Gurney and Sarmousakis[1-4], be described by:

$$\mu^{1/2} = \frac{A\, t(d_i + t)^{3/2}}{d_i} \sqrt{1 + \frac{1}{2}\left(\frac{C}{M}\right)} \qquad (1-4)$$

where:

$2\mu$ = arithmetic average fragment mass (grams)

A = a constant depending on explosive composition and the physical characteristics of the casing material $[\mathrm{gm/in.}^3]^{1/2}$

t and $d_i$ are in inches

$\frac{C}{M}$ = charge-to-metal-mass ratio

CONFIDENTIAL

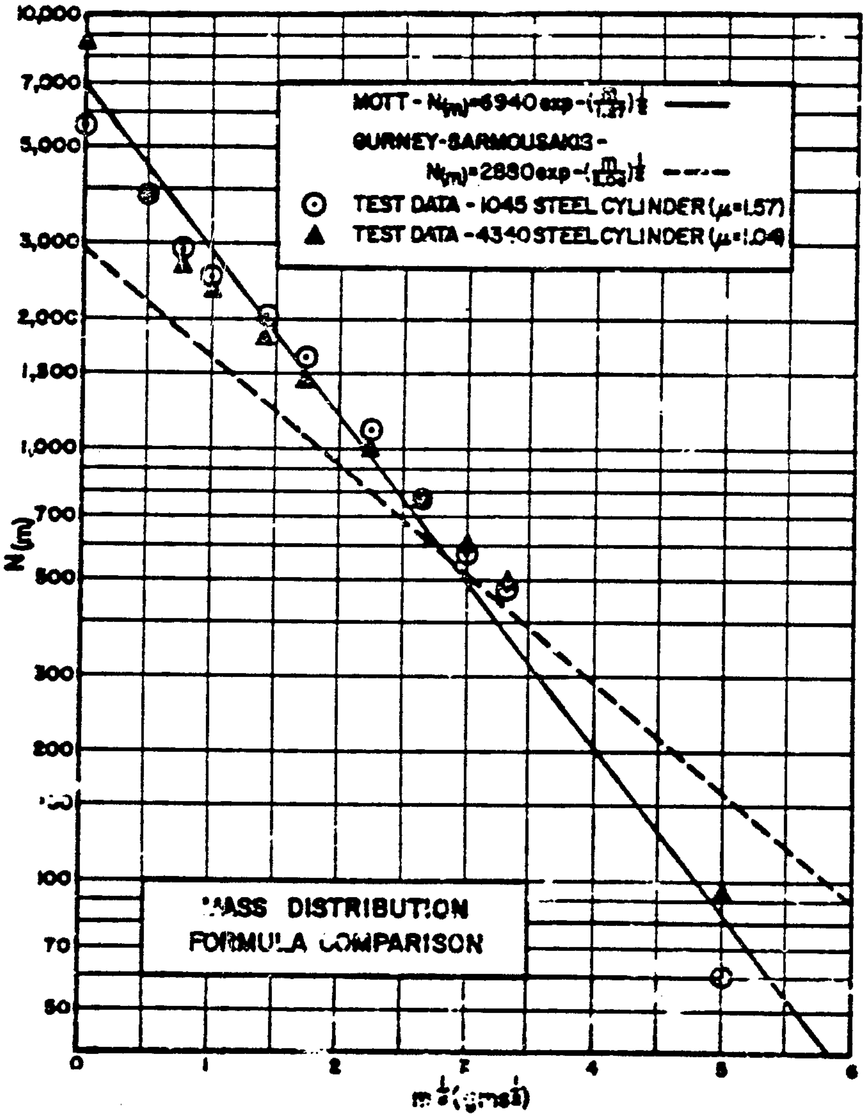


FIGURE 1-1

CONFIDENTIAL

1.2.3 EFFECT OF EXPLOSIVE ON $\mu$. Solem et al of the U. S. Naval Ordnance Laboratory (reference 1-6), experimentally determined values of the Mott scaling constant (B), the Gurney-Sarmousakis scaling constant (A), and the parameter $\mu$ for various explosive compositions. The results obtained from the above experiments are tabulated in Table 1-1 to provide an indication of the effect that various explosives have on $\mu$ as well as the above mentioned scaling constants.

TABLE 1-1 MOTT AND GURNEY-SARMOUSAKIS SCALING CONSTANTS FOR VARIOUS EXPLOSIVES

| Explosive | C/M | $\mu^{1/2}$ - $gms^{1/2}$ | B (1) | A (2) |
|---|---|---|---|---|
| Baratol | 0.562 | 1.237 | 2.73 | 2.55 |
| Comp B | 0.377 | 0.532 | 1.18 | 1.14 |
| Cyclotol (75/25) | 0.380 | 0.471 | 1.05 | 1.01 |
| H-6 | 0.395 | 0.666 | 1.47 | 1.34 |
| HBX-1 | 0.384 | 0.615 | 1.36 | 1.30 |
| HBX-3 | 0.403 | 0.781 | 1.72 | 1.65 |
| Pentolite (50/50) | 0.366 | 0.596 | 1.32 | 1.27 |
| PTX-1 | 0.367 | 0.534 | 1.18 | 1.14 |
| PTX-2 | 0.373 | 0.546 | 1.21 | 1.17 |
| TNT | 0.355 | 0.751 | 1.66 | 1.61 |
| *Comp A-3 | 0.367 | 0.474 | 1.17 | 1.13 |
| *Pentolite (50/50) | 0.363 | 0.631 | 1.41 | 1.27 |
| *RDX/WAX (95/5) | 0.370 | 0.509 | 1.13 | 1.09 |
| *Tetryl | 0.371 | 0.660 | 1.45 | 1.41 |

NOTES: (1) Mott's scaling constant ($gm^{1/2}$ $in.^{-7/6}$)
(2) Gurney-Sarmousakis scaling constant $[gm/in.^3]^{1/2}$
*Indicates pressed explosives

It should be noted that the values of the above constants apply specifically only to cylinders similar to those used in the experiments. The cylinders were made up from AISI 1045 seamless steel tubing with a Rockwell hardness of approximately 100-B. The inside diameter and wall thickness of each cylinder was approximately 2.0 inches and 0.25 inch respectively.

1.2.4 EFFECTS OF CASING MATERIAL ON $\mu$. Only a limited amount of information is available relating the effects that various casing materials have on $\mu$. However, it is concluded in reference 1-7 that:

1. Cylindrical charges utilizing either forged or cast steel, of the types used in current HE shell, produce fragments of a considerably larger average mass than similar charges which employ malleable or ductile cast irons as the casing material.

2. No correlations were found to exist between fragmentation and strength or ductility of the casing material.

The above conclusions are based on results obtained from tests of cylinders which were open at both ends, having an inside diameter of 2.5 inches and a length of 6.0 inches. Three wall thicknesses, 0.2 inch, 0.4 inch, and 0.6 inch were utilized. The three high explosives used for the fragmentation tests were Baratol, TNT and Composition B.

1.2.5 ANGULAR DISTRIBUTION OF FRAGMENTS[1-8]. When a warhead detonates, fragments are projected in many directions. For spherical warheads the density of fragments is substantially constant regardless of direction. However, for cylindrical warheads the greatest density of fragments is contained in a narrow sidespray (commonly referred to as the beamspray) of the order of 20 degrees in width. This beamspray is generally located near 90 degrees from the nose of the warhead as illustrated by Figure 1-2.

Assuming that the warhead under consideration is symmetrical about its longitudinal axis, the number of fragments as a function of the angle $\theta$ measured from the nose of the warhead is described by:

$$N = 2\pi \int_{\theta_1}^{\theta_2} \rho(\theta) \sin \theta \, d\theta \qquad (1\text{-}5)$$

where:

$N$ = number of fragments contained in the polar zone $(\theta_1 - \theta_2)$

$\rho(\theta)$ = number of fragments per steradian in polar zone between $\theta$ and $\theta + d\theta$.

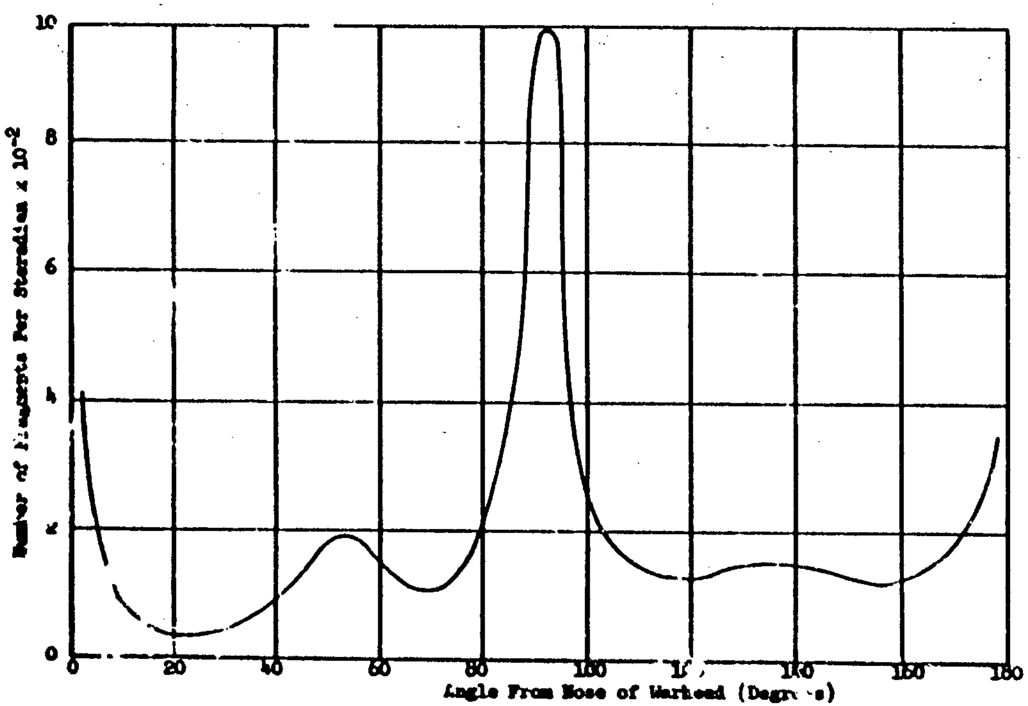


FIGURE 1-2 TYPICAL ANGULAR FRAGMENT DISTRIBUTION

For cylindrical warheads detonated at one end, the position of the fragment beamspray is slightly displaced in a direction away from the point of initiation.[1-9]

The static fragment density $\rho(\theta)$ is usually obtained from proving ground tests, the fragments being collected in fiberboard or other material. When the warhead bursts in flight each fragment has added to its velocity the forward velocity component of the missile at the instant of burst. This shifts the fragment beamspray forward and also increases the density of fragments in the forward hemisphere at the expense of the rear. The equation for making the transformation from static to dynamic conditions is given in reference 1-10 as:

$$\cot \theta_d = \cot \theta + \frac{V_m}{V_f} \csc \theta \qquad (1-6)$$

where:

$\theta_d$ = angle measured from the nose of the warhead (dynamic)

$\theta$ = angle measured from the nose of the warhead (static)

$V_m$ = velocity of the missile

$V_f$ = static velocity of the fragments.

1.2.6 DETERMINATION OF INITIAL FRAGMENT VELOCITY.

1.2.6.1 Theoretical Determination. The Gurney formulas, derived in reference 1-11, have been shown to be quite reliable for predicting the initial velocities of fragments for cylinders and spheres. Based on simple consideration of the explosive energy available, along with the application of the conservation of energy, the prediction of initial velocity of the fragment is given by the following equation:

for cylinders

$$V_o = D\sqrt{\frac{C/M}{1 + 0.5\ (C/M)}} \qquad (1-7)$$

for spheres

$$V_o = D\sqrt{\frac{C/M}{1 + 0.6\ (C/M)}} \tag{1-8}$$

where:

$V_o$ = initial fragment velocity (fps)

D = a constant (fps) depending on the composition of explosive used, GURNEY CONSTANT

C = weight of the explosive charge

M = weight of the fragmenting metal

The above equations neglect the work done in break-up of the metal casing and it is generally agreed that a very small part of the explosive energy is used in this way; hence, the initial fragment velocity depends only on the charge-weight to metal-weight (C/M) ratio and not on the material or construction of the casing.

Values of the Gurney Constant (D), for some of the commonly used explosives, are listed in Table 1-2.

TABLE 1-2 GURNEY CONSTANTS FOR VARIOUS EXPLOSIVES

| Explosive | Gurney Constant D (fps) |
|---|---|
| H-6 | 8,400 |
| Composition B | 8,800 |
| TNT | 7,600 |
| Pentolite | 8,400 |
| HBX | 8,100 |
| Picratol | 7,600 |
| Tritonal | 7,600 |
| Minol-2 | 8,300 |
| Torpex-2 | 8,[illegible] |
| Composition C-3 | 6,800 |

1.2.6.2 Effects of Casing Shape and Thickness on Initial Velocity. Equations (1-7) and (1-8) may be utilized in predicting initial fragment velocity, without serious error, for practically all types of casing material provided that the case is of uniform wall thickness and is either spherical or cylindrical in shape. However, warheads are almost always designed with a variable wall thickness; this is particularly true for projectiles which are extremely thick toward the nose. When conditions such as these exist, the initial velocities of the fragments will vary with respect to the angle from the nose of the warhead. Generally, the velocities are much lower for the nose and base fragments than for beamspray or side fragments. Thus the general practice has been to determine experimentally initial velocity as a function of angle from the nose of the warhead. A typical initial velocity curve is given on Figure 1-3. Although the above equations are quite sensitive to the shape and thickness of the warhead casing, Gurney's formula (Equation (1-7)) for solid cylinders has shown good agreement with experiment for long cylinders (length to diameter ratio of 2.5 and in some cases even for length to diameter ratio of 1.25)[1-10], and moderately good but somewhat high results for short cylinders or ogives.

1.2.6.3 Experimental Determination. The initial velocity of a fragment with known mass, average presented area, and average velocity over a given distance may be approximated by the following equations:

$$V_o = V_{av}\left(\frac{e^w - 1}{w}\right) \qquad (1\text{-}9)$$

where:

$V_o$ = initial velocity of the fragment

$V_{av}$ = average velocity of the fragment

$e$ = base of the natural logarithm

and

$$w = \frac{\rho_a \, C_d \, \bar{A} \, R}{M} \qquad (1\text{-}10)$$

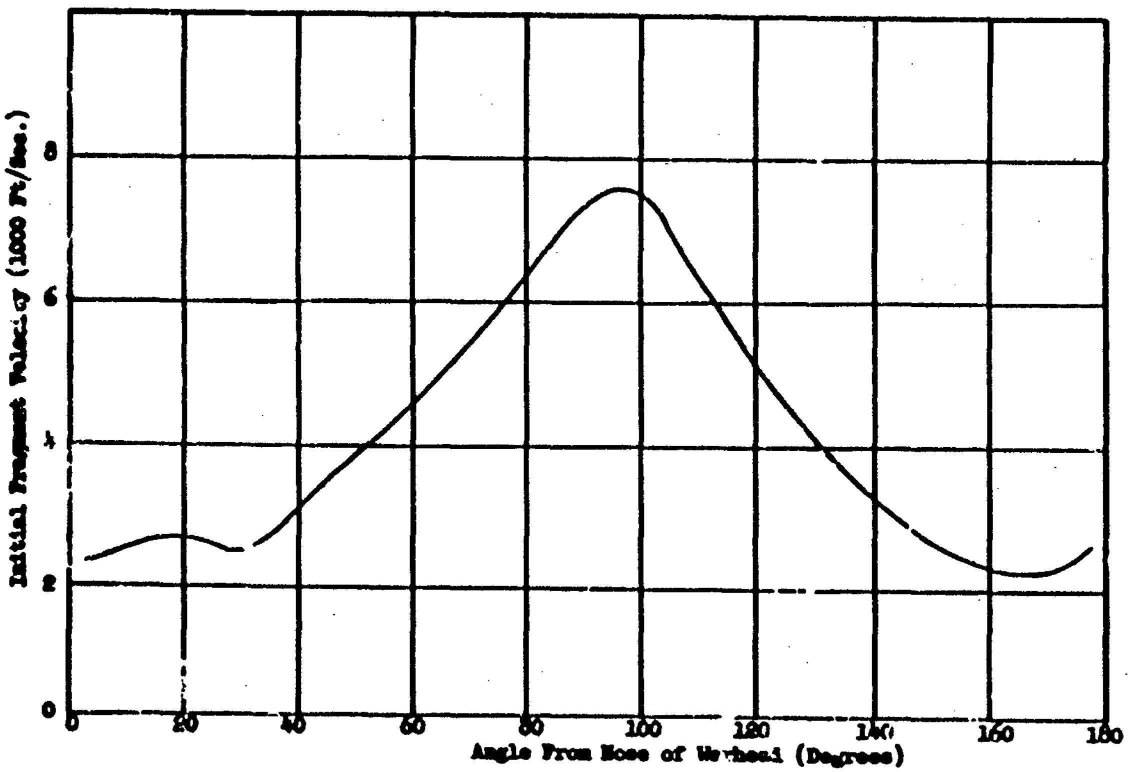


FIGURE 1-3 INITIAL VELOCITY VS ANGLE FROM NOSE

where:

$\rho_a$ = density of the medium

$C_d$ = drag coefficient (dimensionless)

$\bar{A}$ = average presented area of the fragment - see equation (1-11) for a method of determining $\bar{A}$

R = distance over which the average fragment velocity is measured

m = mass of the fragment

Equation (1-9) was obtained by integrating the standard velocity decay equation ($V_R = V_o e^{-w}$), where $V_R$ equals the velocity of the fragment at any distance (R). For a derivation of the velocity decay equation see reference 1-14.

Providing sufficient data are available regarding the average velocity, average presented area, and average mass of fragments produced from a given warhead, an estimated constant initial velocity for a small polar zone may be computed by use of equations (1-9) and (1-10). Here ($V_{av}$) in equation (1-9) is taken as the mean of the average velocities for all fragments in the particular zone. ($\bar{A}$) and (m) in equation (1-10) are taken as the mean average presented area and average mass respectively for all fragments in the particular zone. For an example of the application of this method see reference 1-12. The equation for (w) given in reference 1-12 involves a constant (0.241) which includes the effects of air density and a conversion factor necessary to make (w) dimensionless.

1.2.6.4 Relation Between Mass and Area of Fragments. Equations (1-9) and (1-10) both involve the ratio of the average presented area of the fragment to its mass ($\bar{A}/_m$). If completely random orientation of the fragment is assumed, this ratio is given by the relation

$$\bar{A}/_m = K(m)^{-1/3} \qquad (1\text{-}11)$$

where K is a constant dependent only upon the geometry of the fragment. Table 1-3 gives values of this constant for fragments of various types.

TABLE 1-3 VALUES OF "K" FOR FRAGMENTS OF VARIOUS TYPES

| Type of Fragment | K [1] |
|---|---|
| Random steel fragments | 0.550 |
| Spheres | 0.305 |
| Steel cubes | 0.380 |
| Source reference 1-14. | |

NOTE: [1] m in grams, $\bar{A}$ in sq. cms.

Table 1-4 lists the range of values of K for projectiles of different types. The data presented in Table 1-4 are extracted from reference 1-13.

TABLE 1-4 RANGE OF K FOR FRAGMENT FROM PROJECTILES OF DIFFERENT TYPES

| Type of Projectile | Type of Break-up | Range of K [1] |
|---|---|---|
| Helix of frag. bombs | One-dimensional [2] | 0.422 - 0.486 |
| Medium and large caliber artillery H.E. shell and S.A.P. bombs | Two-dimensional and three-dimensional | 0.486 - 0.553 |
| G.P. bombs, mortar H.E. shells, inner case of frag. bombs; low caliber H.E. artillery shell | Two-dimensional | 0.553 - 0.757 |

NOTES: [1] m in grams, $\bar{A}$ in sq. cms.
[2] This type of break-up could be considered as semi-controlled, since the lateral dimensions of the fragments are fixed by the width and thickness of the rod or wire forming the helix. The other dimension of the fragment is dependent upon the random break-up of the rod material along its longitudinal axis.

1.2.7 TERMINAL FRAGMENT VELOCITY. As fragments travel through the air, they are slowed down by air resistance so that they will strike a stationary target at a velocity lower than their initial velocity. Since their damaging power depends on their terminal (striking) velocity as well as their mass, it is desirable to have a convenient method for determining the variation of striking velocity with such parameters as fragment mass, distance of travel, etc. Such a method is presented in the following paragraph.

If the initial velocity is known, the velocity corresponding to a given distance of travel may be computed by the equation

$$V_R = V_o e^{-w} \qquad (1\text{-}12)$$

where:

$V_R$ = velocity at any distance R

$V_o$ = initial velocity

$w$ = as defined in equation (1-9)

The initial dynamic velocity of the fragments may be obtained by simple vector addition of the fragment initial velocity (static) and the velocity of the missile at the time of detonation of the warhead. This initial dynamic velocity may then be substituted for ($V_o$) in equation (1-12) and the actual terminal velocity of the fragments may be computed.

Although the drag coefficient ($C_d$) is a function of the velocity of the fragment, in the application of equation (1-12) it is usually assumed that $C_d$ is substantially constant over the distance of fragment travel (R). Figure 1-4 gives a plot of $C_d$ as a function of Mach number for various fragment types.

## 1.3 CONTROLLED FRAGMENTATION

An important field of investigation has been that of designing a warhead to produce fragments of a predetermined desirable size. For sufficiently specific warhead/target combinations this is considered desirable, since the control of the size of fragments emitted by a warhead tends to decrease the amount of metal that will be wasted in fragments either too small or too large to be effective.

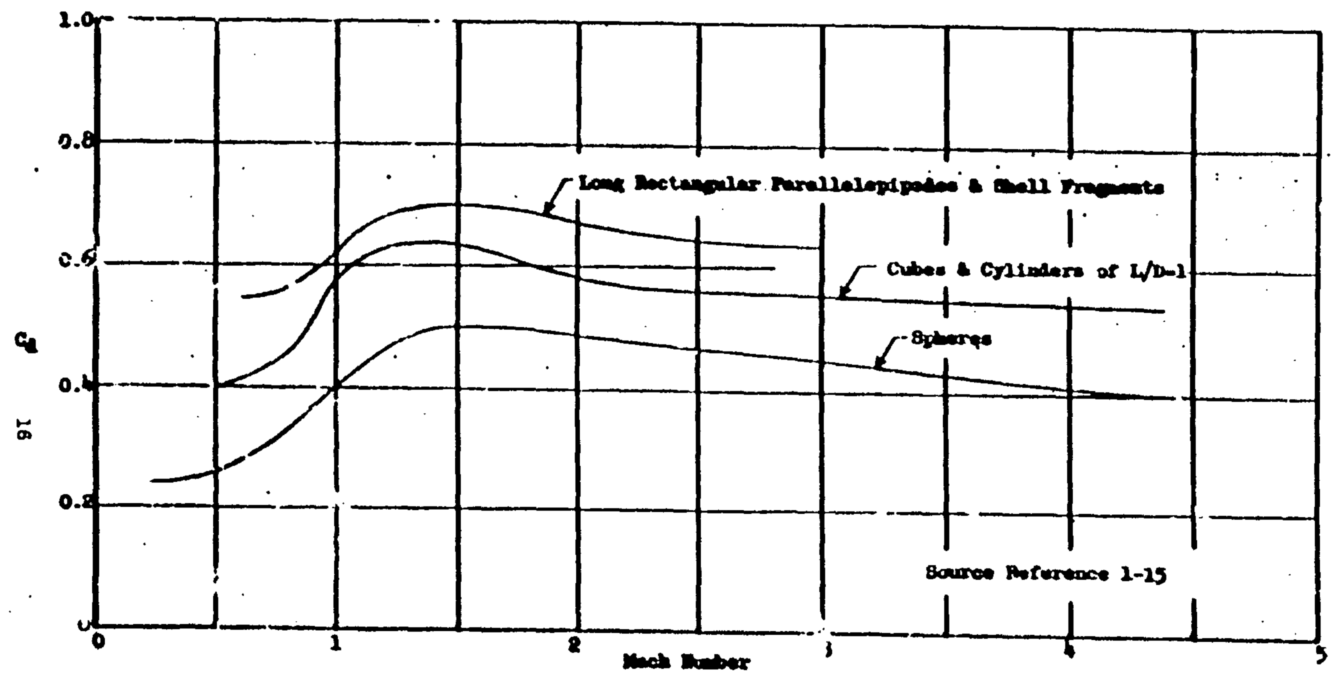


FIGURE 1-4 $C_d$ VS MACH NUMBER FOR VARIOUS FRAGMENT TYPES

1.3.1 METHODS OF FRAGMENT SIZE CONTROL[1-10]. A number of methods are available for controlling the size of fragments such as: (1) preformed or precut fragments, (2) notched or grooved rings, (3) notched or grooved wire, (4) notched casing, (5) multiple walls, and (6) fluted liner. A basic discussion of each of the above methods of controlling fragment size is presented in the following paragraphs.

1.3.1.1 Preformed Fragments. Individual fragments may be cut or formed to the desired size prior to fabricating them onto the warhead. Under this condition the only possible deviation from the initial size would be a result of breakage upon expulsion, adhesion to each other or, possibly, to other parts of the warhead. However, these factors may usually be considered negligible and for all practical purposes nearly 100 percent fragmentation control is achievable.

The principal objection to a wide-scale application of this method of control is that additional structure is required for support of the fragments. This structure usually consists of thin metal inner and/or outer liners, to which the fragments are attached with adhesive, which add to the overall weight but contribute very little to the effectiveness of the warhead. A second objection to preformed fragments is the resulting loss in fragment initial velocity as compared to natural fragmenting warheads. This velocity loss is due to the rupture of the warhead casing early in the expansion. Following the rupture of the casing, the explosive gases escape through the interstices between the fragments and expand to atmospheric pressure, thus decreasing the distance through which the accelerating forces act on the fragments. Recent developments have proven that plastics such as fiberglas laminates may be successfully employed as liner material.

Primary examples to date of applications of the preformed fragment principle are in the fragmentation warheads for the NIKE AJAX, NIKE HERCULES, and HAWK missiles.

1.3.1.2 Notched Rings. In this method of control, a series of notched rings are fitted together to form the warhead casing, each ring thus forming a section of the warhead perpendicular to the axis of symmetry. Essentially, the thickness and width of the rings provide control of two dimensions of the fragments, while notches in the circumference of the ring provide places of weakness where breakage in the third direction is desired.

1.3.1.3 Notched Wire Method. In general this method is similar to the notched rings, discussed in the preceeding paragraph, except that notched wire is wound in a helix or spiral about the warhead casing to control fragmentation.

1.3.1.4 Notched Casing. Instead of notching in one direction and having actual discontinuities in the metal in the other directions (such as in the notched ring or wire method) it is possible to cut, punch, or cast a two dimensional network onto a solid casing. In principle this method is the same as in the notched rings or wire.

1.3.1.5 Multiple Walls. The multiple-wall casings are made by using close-fitted cylinders, each with thickness t/n, where t is the total thickness of the casing and n is the number of walls. This method does not give complete fragmentation control since only the thickness of the fragments is uniform. The effect of using multiple walls has been to reduce the average fragment mass and increase the number of fragments.

1.3.1.6 Fluted Liner Method. In this method the explosive charge is grooved, so that the resulting shaped-charge-effect will break up the casing in the desired places. The charge is grooved by means of the fluted liner (which is sometimes constructed of plastic, wood, or rubber) inserted between the solid metal casing and the explosive. When the warhead is detonated, the flutes give a shaped charge effect which tends to cut the metal casing in the pattern formed by the grooves.

1.4 REFERENCES FOR SECTION 1

1-1. Design for Terminal Effects, Ordnance Corps Pamphlet, ORDP 20-245, May 1957 CONFIDENTIAL
1-2. Fano, U. Data on the Functional Characteristics of Bombs II BRL 493, October 1944, UNCLASSIFIED
1-3. Mott, N. F. A Theory of Fragmentation, AC 3348 (British), January 1943
1-4. Gurney, The Mass Distribution of Fragments from Bombs, Shells, and Grenades, BRL 448, February 1944, CONFIDENTIAL
1-5. Mott, A Theoretical Formula for the Distribution of Weights of Fragments, AC 3642 (British), March 1943
1-6. Solem, Explosives Comparison for Fragmentation Effectiveness, NAVORD Report 2933, August 1953, CONFIDENTIAL

1-7. Abbott, Influence of Mechanical Properties, Casing Thickness and Brisance of Explosive Filler on Fragmentation Characteristics of HE Shell, WAL Report 763/891-1, May 1956, CONFIDENTIAL

1-8. Weiss, Methods for Computing the Effectiveness of Fragmentation Weapons Against Targets on the Ground, BRL 800, January 1952, CONFIDENTIAL

1-9. Lehigh University Bomb Damage Analysis, Final Report LU V.2, Pt. 2, June 1949, UNCLASSIFIED (ASTIA Documents No. ATI 73473)

1-10. Warheads - General, Ordnance Corps Pamphlet ORDP-20-290, July 1959, CONFIDENTIAL

1-11. Gurney, The Initial Velocities of Fragments from Bombs, Shells and Grenades, BRL 405, September 1943

1-12. Portner, Fragmentation Characteristics of the Navy Low Drag Bombs, Mk 81, Mk 82, Mk 83 and Mk 84, NPG Report [illegible], July 1959, CONFIDENTIAL

1-13. Bushkovitch, Presentation Areas of Shell Fragments, BRL 536, April 1945, RESTRICTED

1-14. Giere, Calculating Fragment Penetration and Velocity Data for Use in Vulnerability Studies, NAVORD Report 6621, October 1959, UNCLASSIFIED

1-15. Dunn, Air Drag Measurements of Fragments, BRLM 915, August 1955, CONFIDENTIAL

# SECTION II
# BLAST

## 2.1 BLAST-EXTERNAL

2.1.1 INTRODUCTION. Generally, blast intensity from high explosive ordnance items may be adequately described in terms of two quantities - peak pressure (P) and positive impulse (I). Both quantities vary with distance from the charge and are affected by such parameters as charge composition, charge geometry, casing material, atmospheric pressure and temperature, and Mach wave reflections.

This section provides a brief review of theory, presents experimental data, and compares the two. Much of the work presented in this section has been extracted from the excellent work of Division 2 of the National Defense Research Committee, the Ballistic Research Laboratories and the Naval Ordnance Laboratory, White Oak.

2.1.2 PHENOMENA OF HIGH EXPLOSIVE BLAST IN AIR[2-1].

2.1.2.1 Propagation of the Shock Wave. The rapid expansion of the mass of hot gases resulting from the detonation of an explosive charge gives rise to a wave of compression called a shock wave, which is propagated through the air with a velocity initially much greater than the velocity of sound. As illustrated by Figure 2-1, if the front of the shock wave is considered to be infinitely steep, then the time required for the compression of the undisturbed air ahead of the wave to full shock wave pressure is zero.

For a spherically shaped high explosive charge, the resulting shock wave will be spherical, and since its surface continues to increase as the shock wave travels outward from the charge, the energy per unit area continues to decrease. Thus, the pressure at the wave front, "the peak pressure", also continues to decrease. An additional decrease in pressure may be attributed to attenuation in the form of work done on the air.

Behind the shock-wave front, the pressure in the wave decreases from its initial peak value Near the charge, the pressure in the tail of the wave is greater than one atmosphere. But, as the wave propagates outward from the charge, a rarefaction wave is formed which follows the shock wave. At some distance from the detonation point, the pressure behind the shock wave front falls to a value less than one atmosphere, and then rises again to a steady value equal to one atmosphere. The part of the shock wave in

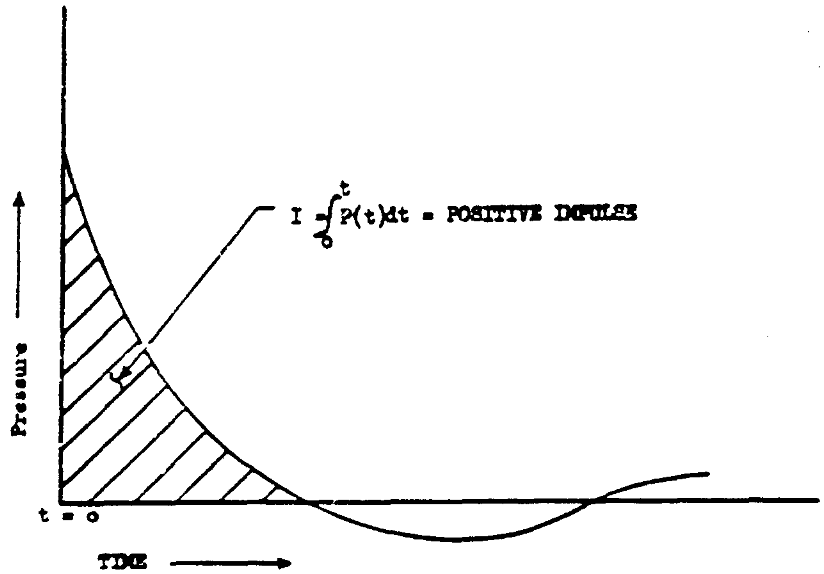


FIGURE 2-1 TYPICAL PRESSURE - TIME CURVE

which the pressure is greater than one atmosphere is called the positive phase, and immediately following it, the part in which the pressure is less than one atmosphere is called the negative or suction phase. For a discussion of the theory of shock waves see reference 2-2.

If the shock wave velocity is known, the peak side-on shock pressure may be obtained from the Rankine-Hugoniot condition

$$\frac{P_s}{P_o} = \frac{2\gamma}{\gamma + 1}\left[\frac{V^2}{C^2} - 1\right] \tag{2-1}$$

where:

$P_s$ = peak side-on pressure
$P_o$ = ambient atmospheric pressure
$V$ = shock velocity in still air
$C$ = sound velocity in air ahead of shock
$\gamma$ = ratio of specific heats (equal to 1.4 for air)

2.1.2.2 Pressure-Time Relationships. A fixed gauge with respect to a charge, which is capable of indicating the side-on pressure instantaneously applied will record pressure in the wave as a function of time. The resulting pressure-time curve is very similar to the curve discussed above and to Figure 2-1. The time elapsing between the arrival of the shock front and the arrival of the part in which the pressure is exactly atmospheric is called the positive duration. An important quantity in the application of blast measurements is the Positive Impulse (I), which is the average pressure during the positive phase multiplied by the positive duration. Mathematically, Positive Impulse may be expressed as

$$I = \int_{0}^{t} P(t)dt \qquad (2-2)$$

where:

t = time of positive duration

P(t) = positive pressure expressed as a function of time.

2.1.2.3 Reflection of Strong Shock Waves. When the pressure in the shock wave is appreciably above one atmosphere, the phenomena may be described in the following manner. In Figure 2-2 there are represented three successive stages in the reflection of strong shocks. The incident wave $I_1$ is first shown as it touches the reflecting surface S. The excess pressure above that of the atmosphere at this point is more than twice that of $I_1$ elsewhere. The magnitude of the increase of pressure over that of $I_1$ is determined by the strength of $I_1$.

As the incident wave expands to some greater $I_2$, the reflected wave $R_2$ also expands, but the reflected wave is not spherical as in the case of very weak shock waves. The angles at which $I_2$ and $R_2$ meet the surface S are not equal, in general, and the angle of the reflected shock $R_2$ depends upon the strength and angle of incidence of the incident shock. It has been found that for each ratio of the pressure in front of the shock wave to that immediately behind the wave front there is a critical angle of incidence beyond which reflection of the type at $R_2$ is impossible. There is some place along the ground where a new type of reflection

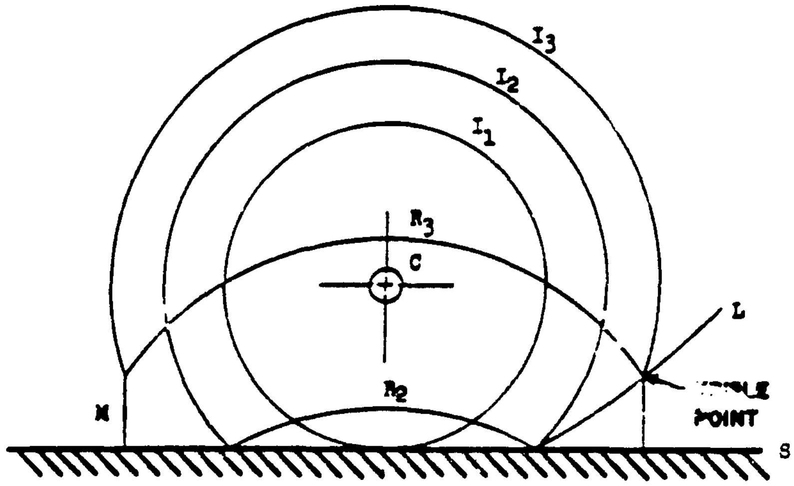


FIGURE 2-2 REFLECTION OF STRONG SHOCK WAVES

called Mach Reflection takes place. The intersection of R and I no longer lies on S, but lies above it and follows some path, L. A new wave M, the Mach wave, connects the intersection of R and I to the surface. The intersection of the incident wave, the reflected wave, and Mach wave is called the triple point.

As the phenomenon progresses, the Mach wave grows and the triple point describes a curve through the air. The geometry of the Mach reflection phenomenon has been studied, with particular reference to the path followed by the triple point, by various investigators. Empirical methods of analyzing blast data and methods for expressing the height of the triple point as a function of distance are reported in reference 2-3. Typical paths for several charge heights and weights are shown on Figure 2-3.

As the Mach wave grows in height, it absorbs the incident and reflected waves. Ultimately, at distances very large compared to heights of burst, the whole configuration of shocks becomes approximately a single spherical shock wave intersecting the ground orthogonally.

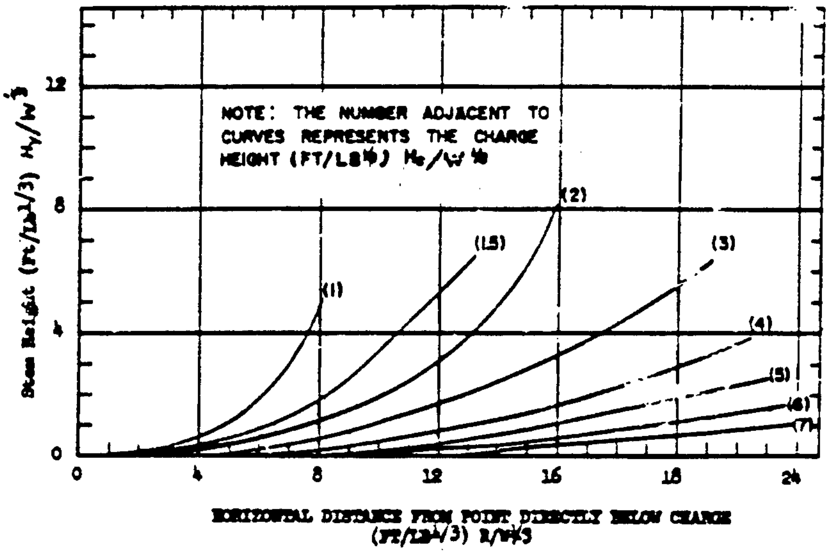


FIGURE 2-3 MACH STEM HEIGHT VS HORIZONTAL DISTANCE FROM CHARGE FOR VARIOUS CHARGE HEIGHTS FOR TNT

2.1.2.4 __Effects of Charge Shape and Orientation__[2-4]. The orientation of non-spherical charges relative to the gauge has a significant effect on the intensity of the measured shock pressure and impulse, since the shock configuration from such charges is of a complex nature. For example, bridge waves resembling Mach waves form off the edges of cylindrical charges and the pattern some time after emergence takes the form illustrated by Figure 2-4.

Assymetry is not the only cause of complications in wave patterns, for even in spherical explosions away from all reflecting surfaces the gauges indicate the existence of secondary and tertiary shocks. However, in measurements off spheres and off sides of cylinders, these secondary shocks are small relative to the primary wave. Hence, measurements of impulse in these cases usually exclude the contributions of these secondary shocks. In measurements off ends of cylinders and Engineers' demolition blocks,

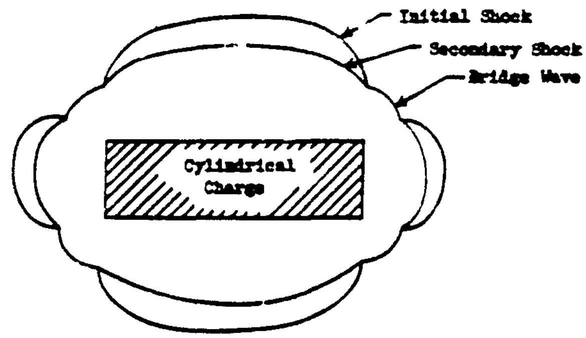


FIGURE 2-4 CYLINDRICAL CHARGE WAVE PATTERN

however, secondary peaks are large and occur well within the initial positive phase, as illustrated by Figure 2-5. Therefore, the impulse data include the area below the secondary peaks.

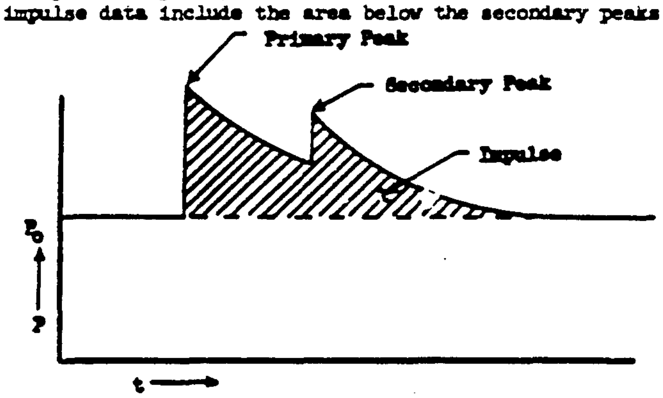


FIGURE 2-5 WAVE FORM OFF BASE OF CYLINDERS[2-4]

The second shock is at times as intense as the first shock, particularly in the case of charges with $L/D =$ [illegible]. Peak pressure in such cases is the pressure of the first shock, while impulse is taken to be the entire area of the pressure-time curve above the ambient level ($P_o$).

Figures 2-6 and 2-7 from reference 2-4 compare the pressure and impulse curves for cylindrical and spherical charges of Composition B. Generally the results presented in reference 2-4 indicate that the initial intensities for spheres are lower than cylinders.

### 2.1.3 THE VARIATION OF PEAK PRESSURE AND POSITIVE IMPULSE WITH DISTANCE FROM THE CHARGE

2.1.3.1 Theory. In the study of explosions and the shock waves resulting from them, one of the most important and at the same time, one of the most difficult problems was to understand the laws that govern the propagation of shock through the air. In 1944, a theoretical solution to the one dimensional spherical blast problem was devised by Kirkwood and Brinkley (references 2-5 and 2-6). Basically, Kirkwood and Brinkley transformed the non-linear hydrodynamic equations into a set of ordinary partial differential equations, which, together with (1) the Rankine-Hugoniot relationships and (2) an assumed energy-time curve, made it possible to obtain approximate space-time values of the blast pressure and positive impulse.

2.1.3.2 Verification of Theory. The Kirkwood-Brinkley theoretical results have been verified to a surprising degree over a wide range of variables. As shown on Figures 2-8, 2-9, 2-10 and 2-11, excellent agreement exists between the experimental points of Fisher and Weibull (references 2-7 and 2-8) and the theoretical curves calculated by Kirkwood and Brinkley. The theoretical curves for TNT and Pentolite are based on the assumed values of 1060 cal/g and 1450 cal/g as the energy of detonation. The better general agreement is found for TNT but that for Pentolite is by no means considered poor. The peak pressure-distance curves exhibit the best agreement between theory and experiment, probably because the peak pressure is a relatively insensitive function of the energy-time relationship assumed The impulse curves show greater discrepancies, however, because they are significantly more sensitive to this relationship.

2.1.3.3 Empirical Formulae. The side-on excess peak pressures and positive impulses of air shock waves from detonations of spherically shaped explosives charges of 50/50 Pentolite have been measured by BRL (reference 2-13) under ambient atmospheric pressures and temperatures simulating altitudes up to 50,000 feet. The reduction in peak pressure and positive impulse attendant on

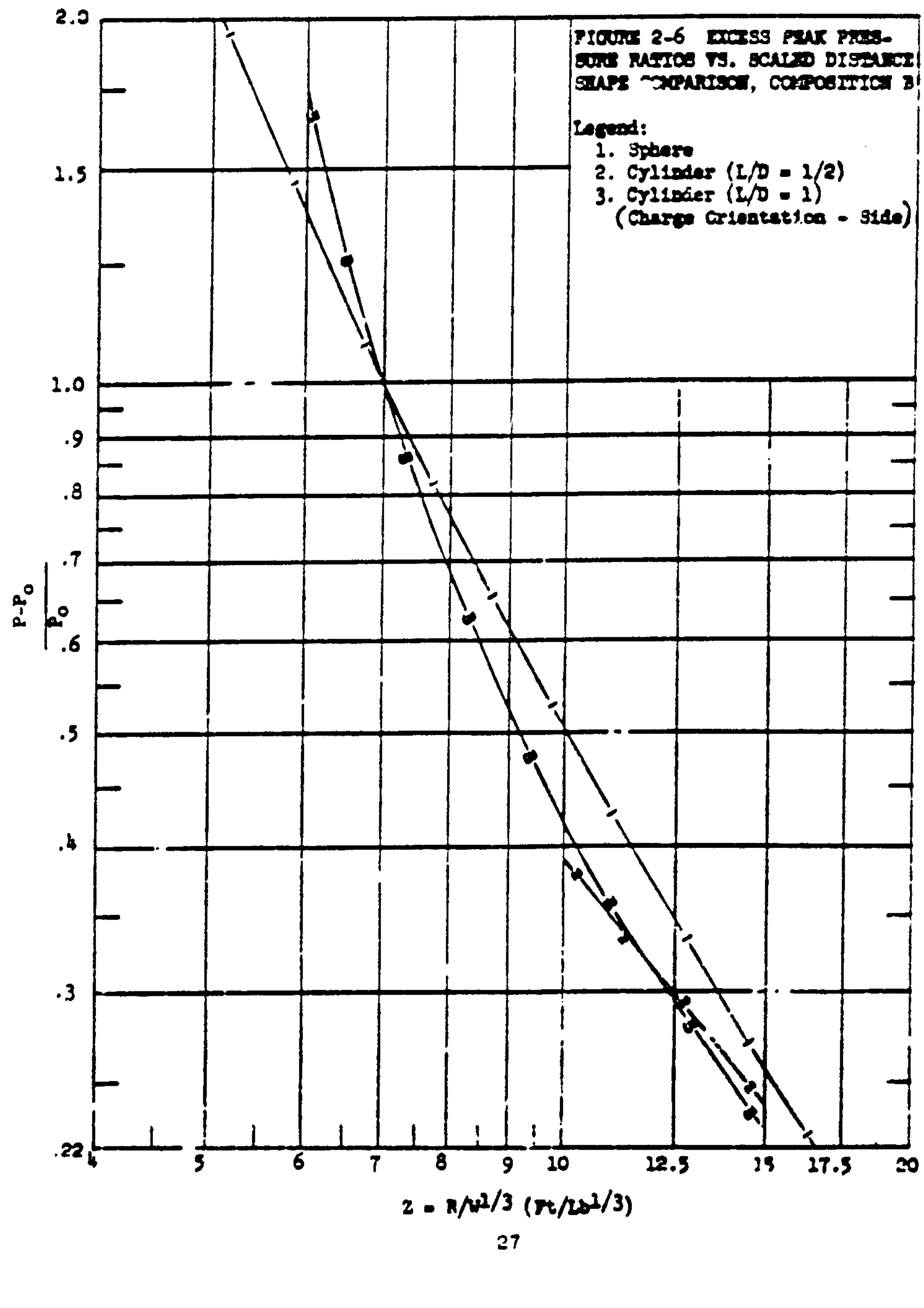

FIGURE 2-6 EXCESS PEAK PRESSURE RATIOS VS. SCALED DISTANCE SHAPE COMPARISON, COMPOSITION B
Legend:
1. Sphere
2. Cylinder (L/D = 1/2)
3. Cylinder (L/D = 1)
(Charge Orientation - Side)
2.0
1.5
1.0
.9
.8
.7
.6
.5
.4
.3
.22
4
5
6
7
8
9
10
12.5
15
17.5
20
$\frac{P-P_o}{P_o}$
$Z = R/W^{1/3}$ (Ft/Lb$^{1/3}$)

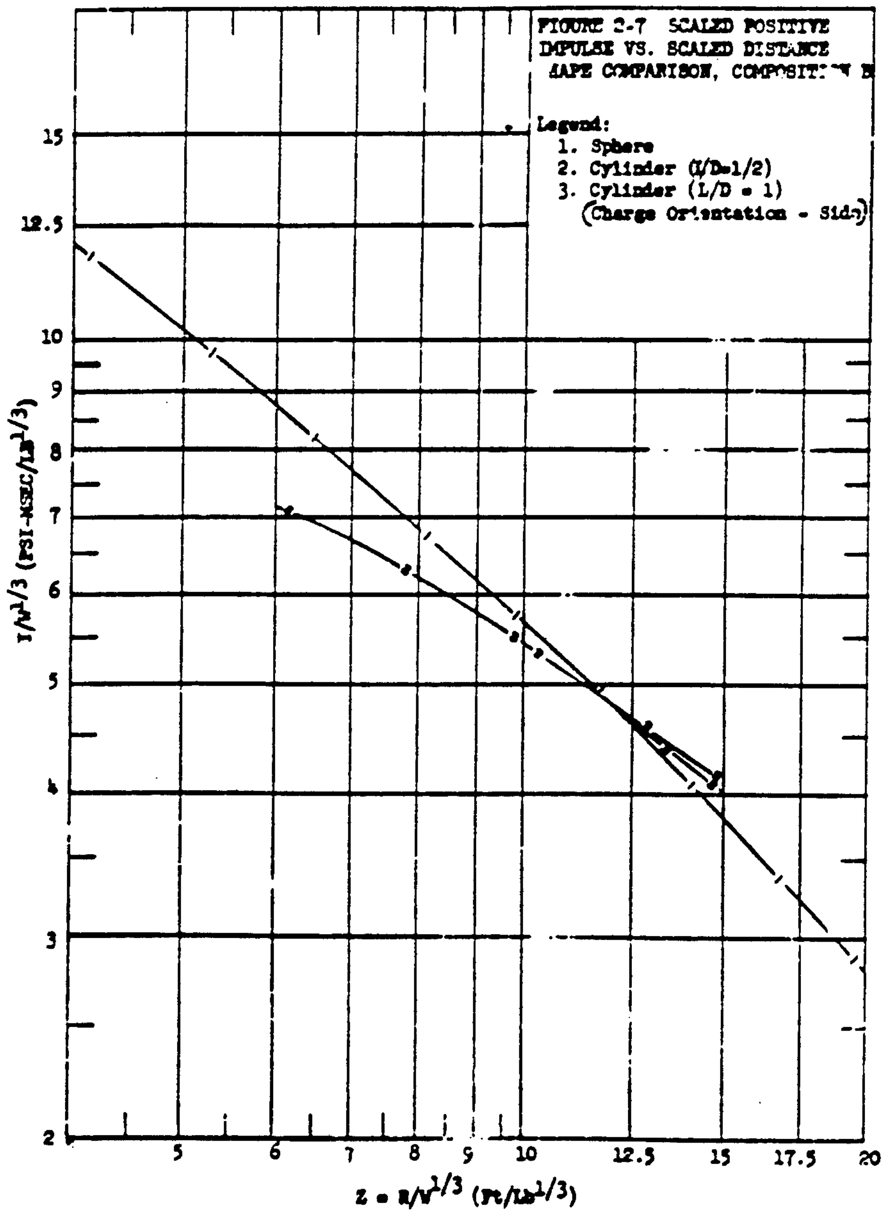


FIGURE 2-7 SCALED POSITIVE IMPULSE VS. SCALED DISTANCE SHAPE COMPARISON, COMPOSITION B

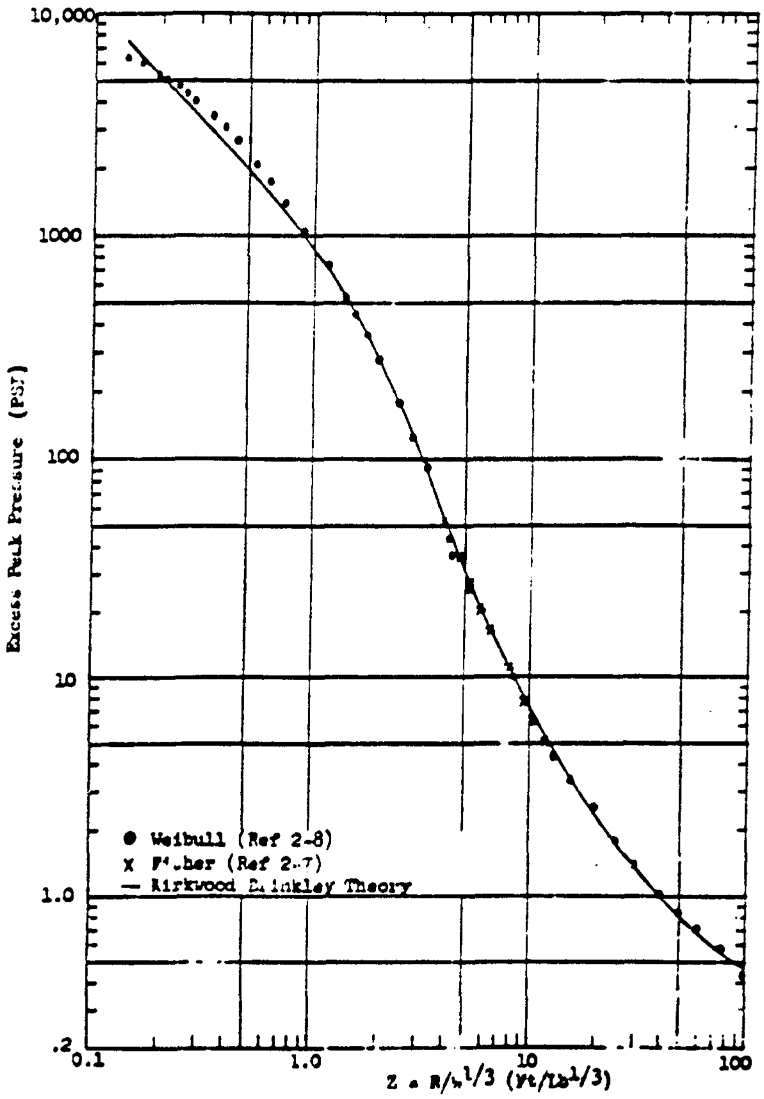


FIGURE 2-8 EXCESS PEAK PRESSURE VS SCALED DISTANCE FOR SPHERICAL TNT IN FREE AIR AT SEA LEVEL

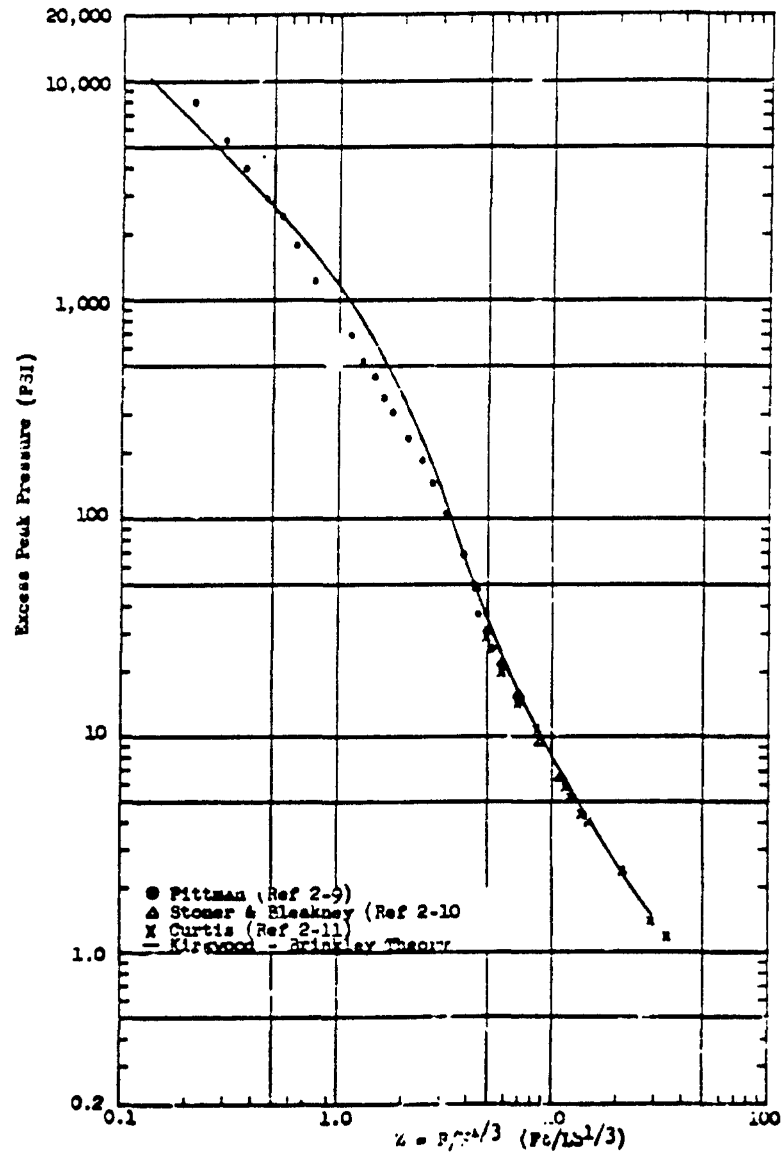


FIGURE 2-9 EXCESS PEAK PRESSURE VS SCALED DISTANCE FOR SPHERICAL PENTOLITE IN FREE AIR AT SEA LEVEL

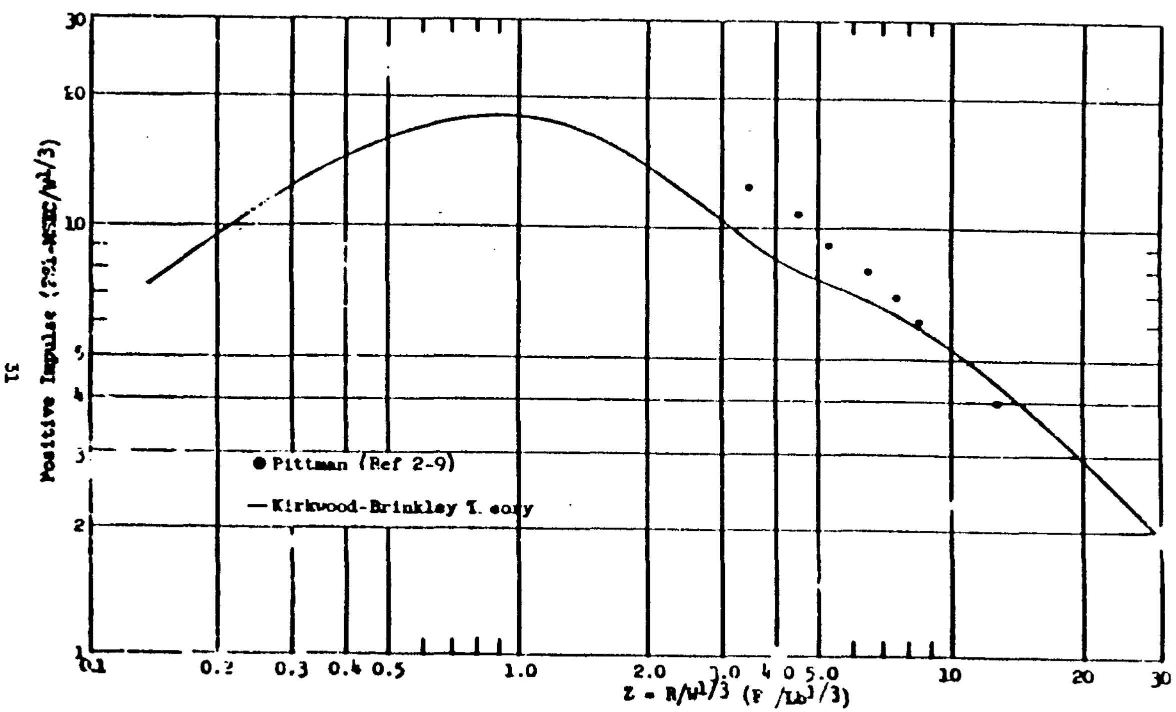


FIGURE 2-10 SCALED POSITIVE IMPULSE VS SCALED DISTANCE FOR SPHERICAL TNT IN FREE AIR AT SEA LEVEL

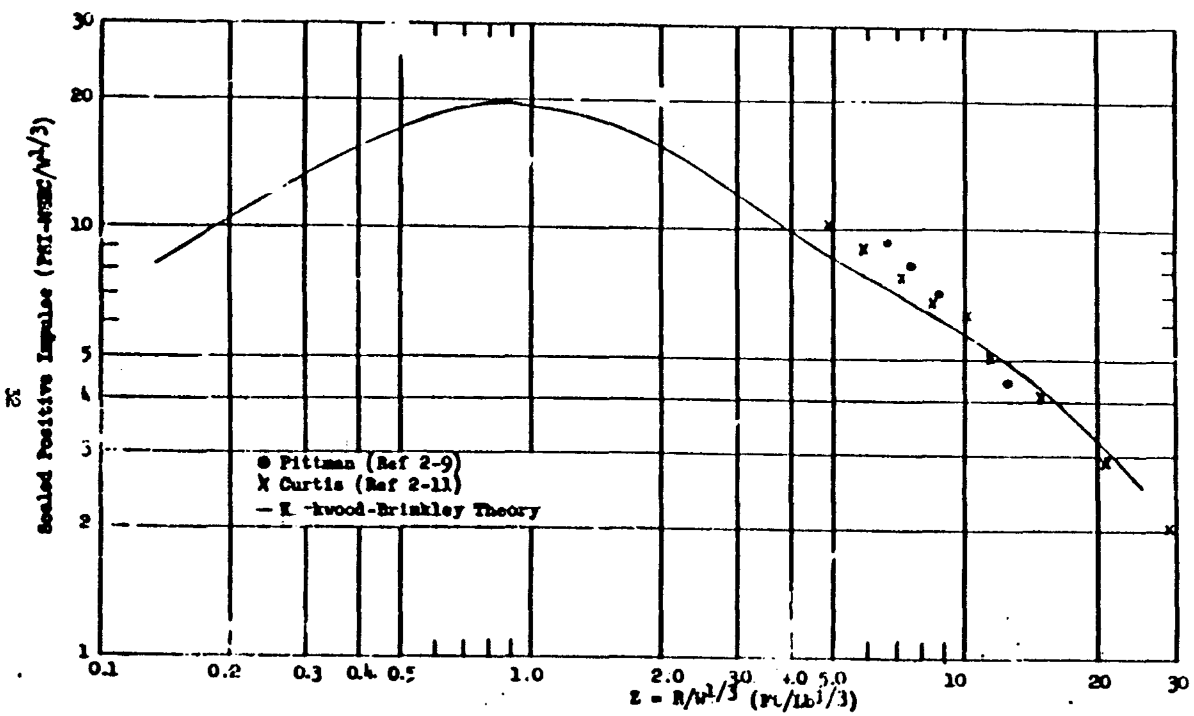


FIGURE 2-: SCALED POSITIVE IMPULSE VS SCALED DISTANCE FOR SPHERICAL PENTOLITE IN FREE AIR AT SEA LEVEL

decrease in ambient pressure for values of $Zp_o^{1/3}$ ranging from approximately 2 to 30 can be expressed by the following equations derived from BRL experimental data.

For peak pressure:

$$\frac{p}{p_o} = \frac{37.95}{Zp_o^{1/3}} + \frac{154.9}{(Zp_o^{1/3})^2} + \frac{203.4}{(Zp_o^{1/3})^3} + \frac{403.9}{(Zp_o^{1/3})^4} \qquad (2\text{-}3)$$

For positive impulse:

$$\log_{10} \frac{I}{p_o^{2/3}\, W^{1/3}} = 1.374 - 0.695 \log_{10} (Zp_o^{1/3}) \qquad (2\text{-}4)$$

where:

$p$ = peak pressure in psi

$p_o$ = ambient atmospheric pressure in atmospheres (1 atmosphere = 14.7 psi)

$Z = R/W^{1/3}$

R = distance from explosive in feet

W = weight of explosive in pounds

I = positive impulse in psi milliseconds.

Equations (2-3) and (2-4), above, may be applied to other explosives through the use of applicable relative peak pressure and positive impulse values. Table 2-1 summarizes the peak pressure and positive impulse values of several explosives relative to TNT (references 2-14 and 2-15).

2.1.4 CASING EFFECTS ON BLAST

2.1.4.1 Functions of the Warhead Case. Weapons, when put into service, normally employ some type of casing around the high explosive charge. The function of the case depends upon whether the warhead is designed to be detonated inside or outside of the target envelope, that is whether blast is internal or

TABLE 2-1 CHARACTERISTICS OF EXPLOSIVES

| Explosive | Composition | Peak Pressure EW (1) | Peak Pressure EV (2) | Peak Pressure EW (1) | Peak Pressure EV (2) | Experimental Density (gm/cc) |
|---|---|---|---|---|---|---|
| Composition B | 60/40:RDX/TNT | 1.13 | 1.21 | 1.06 | 1.13 | 1.68 |
| TNT | TNT | 1.00 | 1.00 | 1.00 | 1.00 | 1.48 |
| H-6 | 47/31/22/5:RDX/TNT/AL/Wax | 1.27 | 1.44 | 1.38 | 1.57 | 1.74 |
| HBX-1 | 42/40/18/5:RDX/TNT/AL/Wax | 1.21 | 1.36 | 1.21 | 1.36 | 1.72 |
| HBX-3 | 32.7/30.5/36.8/5:RDX/TNT/AL/Wax | 1.16 | 1.39 | 1.25 | 1.49 | 1.82 |
| Pentolite | 50/50:TNT/PETN | 1.19 | 1.18 | 1.07 | 1.10 | 1.52 |
| Tritonal | 80/20:TNT/AL | 1.07 | 1.17 | 1.11 | 1.25 | 1.74 |
| Picratol | 52/48 EXPL D/TNT | 0.90 | 0.92 | 0.93 | 0.95 | 1.51 |
| Minol-2 | 40/40/20:TNT/$NH_4NO_3$/AL | 1.24 | 1.41 | 1.22 | 1.37 | 1.68 |
| Explosive D | 97/3 AMM Picrate/Misc | 0.85 | 0.86 | 0.81 | 0.82 | 1.49 |
| Composition A-3 | 91/9 RDX/Wax | 1.09 | 1.16 | 1.07 | 1.14 | 1.53 |

(1) Equivalent weight
(2) Equivalent volume

external to the target. The casing for an internal blast warhead must function not only as a container for the explosive charge but also as a means for penetrating the target. The case for an external blast warhead serves primarily as a container for the charge. Considering both internal and external blast warheads, a secondary purpose of the casings is the potential damage capability as a result of case fragmentation.

2.1.4.2 Fano Formula[2-16]. The steel case retaining an explosive charge reduces the blast effectiveness of the charge, since energy is required to accelerate the casing after detonation has been accomplished. The effect of this was first studied by Fano of [illegible] who produced the following formula:

$$\frac{W'}{W} = 0.2 + \frac{0.8}{1 + \frac{2M}{C}} \quad \text{for peak pressure and positive impulse} \qquad (2\text{-}5)$$

This equation was developed through the extension of the work of Gurney who considered the kinetic energy at the time of rupture as being made up of the kinetic energy of the explosion produced gases and the kinetic energy of the case.

Later investigations of casing effects on blast at the Naval Ordnance Laboratory, reference 2-16, yielded the following empirical relations.

For positive impulse:

$$\frac{W'}{W} = \frac{1 + \frac{M}{C}(1 - M')}{1 + \frac{M}{C}} \qquad (2\text{-}6)$$

For peak pressure:

$$\frac{W'}{W} = 1.19\left[\frac{1 + \frac{M}{C}(1 - M')}{1 + \frac{M}{C}}\right] \qquad (2\text{-}7)$$

where:

$W'$ = equivalent bare charge weight

$W$ = actual charge weight

$M$ = case weight in cylindrical section

$C$ = charge weight in cylindrical section

$M' = M/C$ when $M/C < 1$

$M' = 1$ when $M/C > 1$

2.1.4.3 British Formulae. A relatively recent series of casing effects tests was conducted by the ARDE (reference 2-[illegible]), which utilized 66 pound cylindrical charges of RDX/TNT (60/40) and Minol-2 (40% TNT/40% Ammonium nitrate/20% Aluminum). The charge weight to total weight ratios, $\frac{C}{C + M} = A$, ranged from .05 to 1. Utilizing data from these tests, ARDE developed the following empirical relations.

For non-aluminized explosives:

$$\frac{W'}{W} = \frac{.8 + .2A}{2 - A} \quad \text{for peak pressure} \qquad (2\text{-}8)$$

and

$$\frac{W'}{W} = \frac{.4 + .6A}{2 - A} \quad \text{for positive impulse} \qquad (2\text{-}9)$$

It should be noted that the British formula for positive impulse (equation 2-9) is the same as the Fano formula (equation 2-5).

For aluminized explosive:

$$\frac{W'}{W} = \frac{1.10 - 0.10A}{2 - A} \quad \text{for peak pressure and positive impulse} \qquad (2\text{-}10)$$

2.1.4.4 Comparison of Formulae. A graphical comparison of the NOL/WO formulae with the British Formulae is shown in Figure 2-12. Regarding non-aluminized explosives it is evident that both Fano and ARDE results (equations 2-5 and 2-9) agree for positive impulse but are lower than NOL/WO results (equation 2-6) for values of "A" greater than 0.4. The British results for peak pressure (equation 2-8) are considerably higher than the NOL/WO revised formula (equation 2-7) for peak pressure for values of "A" less than 0.5.

Regarding aluminized explosives, the curve (equation 2-10) indicates an increase in both peak pressure and positive impulse over that obtained for comparable weights of non-aluminized explosives.

Based on results available in the references and on the graphical comparison of the above formulae it is suggested that:

1. Equation 2-10 be used for peak pressure and positive impulse for aluminized explosives.

2. Either equation 2-5 or 2-9 be used for positive impulse for non-aluminized explosives.

3. Equation 2-8 be used for peak pressure for non-aluminized explosives.

2.1.5 EXPERIMENTAL MACH REFLECTION STUDIES

The reflection of shock waves at oblique angles of incidence upon surfaces of hard packed clay soil and water has been studied by NOL in reference 2-18. Peak pressure information was obtained in the far Mach region along the reflecting surface by the shock velocity method. A perfectly rigid reflecting surface was simulated by the intersection of shock waves from two identical spherical charges fired simultaneously.

2.1.5.1 Mach Reflection Coefficients. The effects of each type of reflecting surface, reported in the above studies, are expressed as reflection coefficients. The coefficients are given as the ratio of weight of explosive necessary to be fired in free air to that fired near the reflecting surface to produce the same pressure at the same radial distance. Results of these studies are presented in Table 2-2 as a function of reduced charge height above reflecting surface ($h/W^{1/3}$) in ($ft/lb^{1/3}$).

CONFIDENTIAL

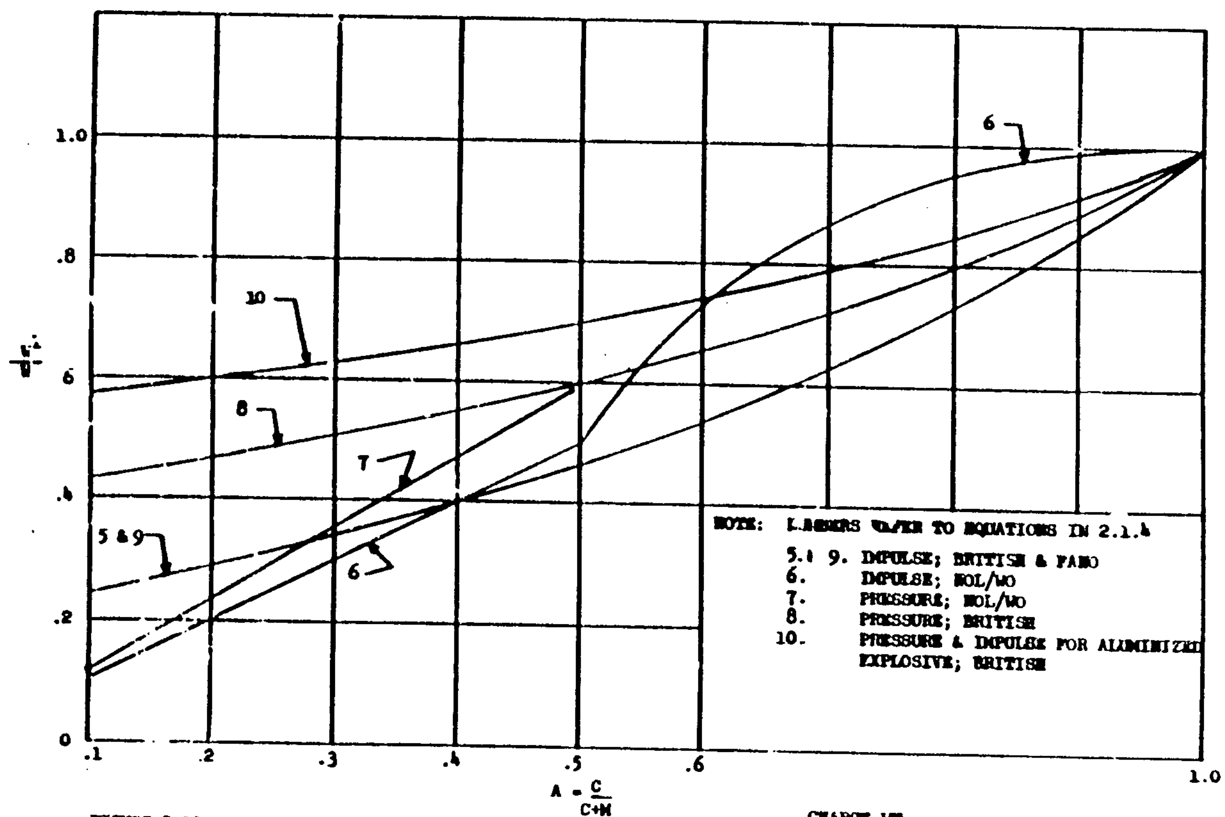


FIGURE 2-12 EQUIVALENT BARE CHARGE WT./ACTUAL CHARGE WT. VS $\frac{\text{CHARGE WT.}}{\text{CHARGE WT. + METAL WT.}}$

TABLE 2-2 REFLECTION COEFFICIENTS

| Charge | $h/W^{1/3}$ | Reflector | Reflection Coefficient |
|---|---|---|---|
| 8-lb TNT | 2.14 | Hard Clay | 1.87 |
| 8-lb TNT | 0.88 | Hard Clay | 1.88 |
| 8-lb TNT | 0.62 | Hard Clay | 1.79 |
| Two 8-lb TNT Charges | 2.14 | Perfect Reflector | 2.06 |
| Two 8-lb TNT Charges | 0.62 | Perfect Reflector | 1.95 |
| Two 8-lb TNT Charges | 0.55 | Perfect Reflector | 1.97 |
| 1-lb Pentolite | 1.50 | Water | 1.91 |

### 2.1.6 APPLICATION

2.1.6.1 Free Air Blast Estimates. The estimation of peak pressure and positive impulse for specific warheads may be accomplished through the application of the preceding formulae and data presentations. For example, the expected free-air blast pressure and positive impulse of the MARK 81 Low Drag Bomb could be estimated through the use of the equation and curves given in sections 2.1.3 and 2.1.4. Based on the geometrical dimensions and explosive characteristics of the bomb, an equivalent bare charge weight ($W'$) would be computed through the use of equation 2-10. The resulting weight would then be adjusted to an equivalent weight of an explosive for which empirical pressure and impulse versus reduced distance ($R/W^{1/3}$) data exist. Knowing the equivalent free air bare charge weight, the pressure or impulse at a given distance R may be read directly from an empirical curve such as Figures 2-8 and 2-10.

2.1.6.2 Mach Region Blast Estimates. Estimates of the blast pressure and impulse, under conditions where the target or gauge would be positioned within the Mach region (see Figure 2-13) may be made in a manner similar to that described previously for free-air. However, it would first be neccessary to make an additional adjustment to the equivalent bare charge weight to account for Mach wave reflection. The equivalent bare charge weight in the Mach region would be obtained by multiplying the $W'$ obtained for free-air by an applicable reflection coefficient. Values for various reflecting surfaces may be obtained from Table 2-2.

Knowing the equivalent bare charge weight in the Mach region, the pressure and impulse at a given distance R could be read directly from empirical curves as described previously for free air.

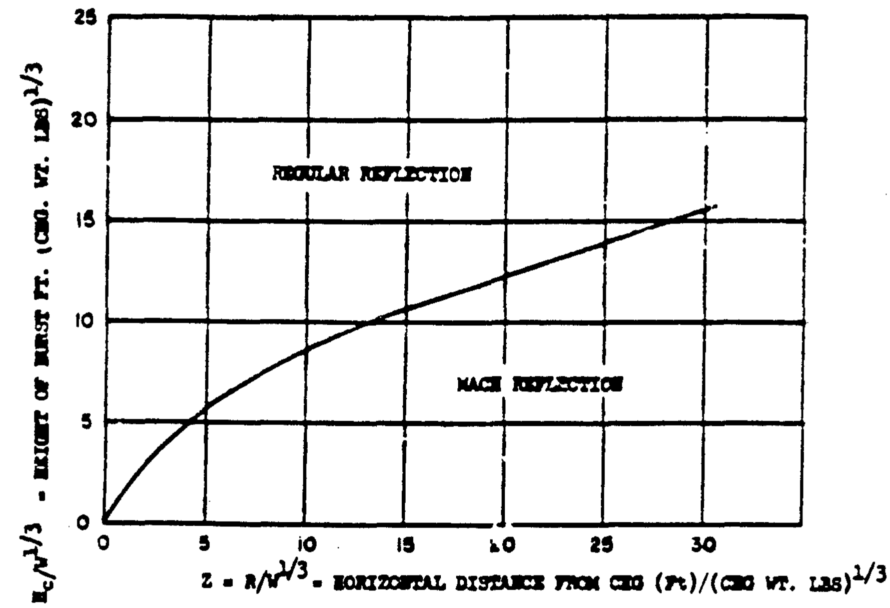


FIGURE 2-13 CONDITIONS FOR MACH REFLECTION

2.1.6.3 Conversion from Side-on to Face-on Pressure[2-18]. To apply experimental or theoretical side-on peak pressure results it is first necessary to convert to expected face-on pressures at the target reflecting surface. By assuming the shock wave to be spherically symmetric, the face-on pressure $P_r$ at the reflecting surface may be inferred using the relation

$$\frac{P_r}{P_s} = 2 + \frac{6\frac{P_s}{P_0}}{\frac{P_s}{P_0} + 7} \qquad (2\text{-}11)$$

where:

$P_s$ = excess side-on pressure

$P_o$ = ambient atmospheric pressure.

Figure 2-14 presents experimentally derived curves relating scaled side-on and face-on impulse to scaled distance for 1/2 to 8-lb spherical Pentolite 50/50 charges. These curves may be used to estimate the expected positive impulse at the reflecting surface.

## 2.6 REFERENCES FOR SECTION 2

2-1. Effects of Impact and Explosion, Summary Technical Report of Division 2, NDRC, Vol. 1, 1946, CONFIDENTIAL

2-2. Cole, Underwater Explosions, Princeton University Press, 1948, UNCLASSIFIED

2-3. Halverson, The Effects of Air Burst on the Blast from Bombs and Small Charges, OSRD 4899, NDRC A-320, April 1945, UNCLASSIFIED

2-4. Makino, R. C. and Goodman, H. J., Air Blast Data on Bare Explosives of Different Shapes and Compositions (U), BRLM 1015, June 1956, CONFIDENTIAL

2-5. Kirkwood and Brinkley, A New Theory of Shock Wave Propagation with and Application of the Shock Wave Produced in Air by the Explosion of Cast Pentolite, OSRD 4275f, AES-3f, October 1944, UNCLASSIFIED

2-6. Kirkwood and Brinkley, Theory of Propagation of Shock Waves from Explosive Sources in Air and Water, OSRD 4814, NDRC A-318, March 1945, UNCLASSIFIED

2-7. Fisher, Spherical Cast TNT Charges; Air Blast Measurements on, NOLM-10780, January 1950, UNCLASSIFIED

2-8. Weibull, Explosion of Spherical Charges in Air: Travel Time, Velocity of Front, and Duration of Shock Waves, BRL Translation Report X-127, February 195[illegible], UNCLASSIFIED

2-9. Pittman, Close-in Air Blast Measurements from Explosions of Bare and Rubber-Cased 473-Gram Spherical Pentolite Charges, NAVORD Report 4[illegible]72, April 1957, CONFIDENTIAL

2-10. Stoner and Bleakney, Attenuation of Spherical Shock Waves in Air, J. Appl. Phys., Vol. 1[illegible](7), July 19[illegible]. UNCLASSIFIED

2-11. Curtis, Free Air Blast Measurements on Spherical Pentolite, BRLM-544, July 1951, UNCLASSIFIED

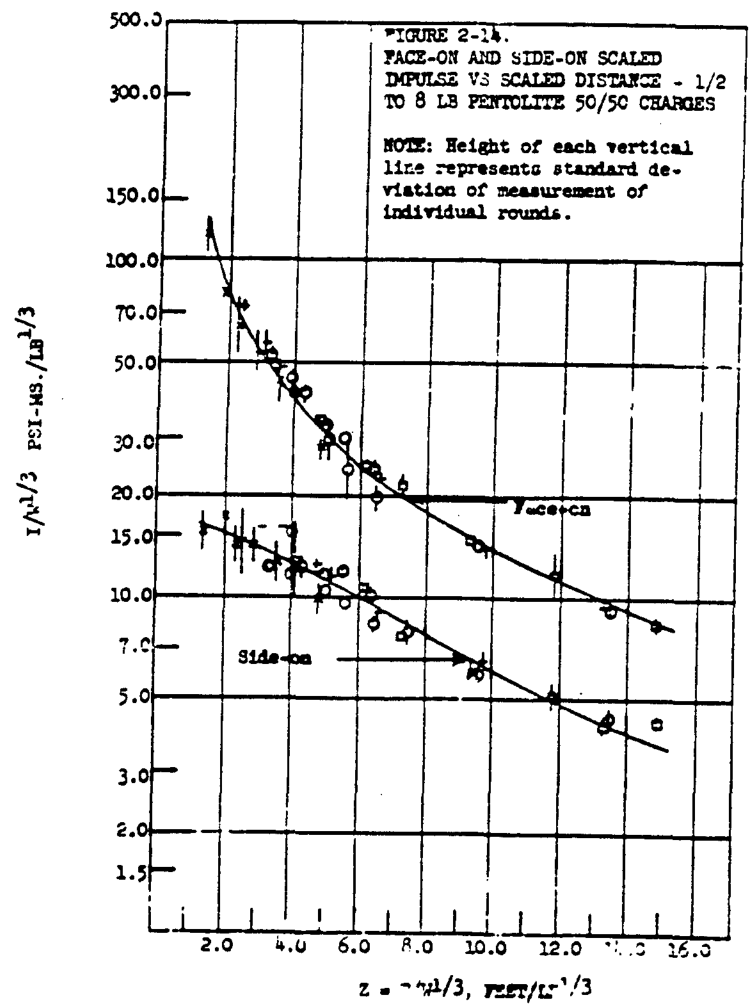
FIGURE 2-14.
FACE-ON AND SIDE-ON SCALED IMPULSE VS SCALED DISTANCE - 1/2 TO 8 LB PENTOLITE 50/50 CHARGES
NOTE: Height of each vertical line represents standard deviation of measurement of individual rounds.
500.0
300.0
150.0
100.0
70.0
50.0
30.0
20.0
15.0
10.0
7.0
5.0
3.0
2.0
1.5
Face-on
Side-on
2.0
4.0
6.0
8.0
10.0
12.0
16.0
PSI-MS./LB1/3
FEET/LB1/3

2-12. Fisher and Pittman, Air Blast Resulting from Detonation of Small TNT Charges, NAVORD Report 2890, July 1953, UNCLASSIFIED

2-13. Dewey and Sperrazza, The Effects of Atmospheric Pressure and Temperature on Air Shock, BRL 721, May 1950, UNCLASSIFIED

2-14. Christian and Fisher (Editors), Explosion Effects Data Sheets, NAVORD Report 2986, originally published June 1955, with subsequent revisions through March 1959, CONFIDENTIAL

2-15. Fisher, The Determination of the Optimum Air Blast Mixture of Explosives in the RDX/TNT/Aluminum System, NAVORD Report 2348, March 1952, CONFIDENTIAL

2-16. Fisher, The Effects of the Steel Case on the Air Blast from High Explosives, NAVORD Report 2753, February 1953, CONFIDENTIAL

2-17. Reduction of Excess Blast Pressure and of Positive Blast Impulse Intensity for Cased Charges of RDX/TNT 6[illegible] and of Minol 2, ARDE Report of March 1955, CONFIDENTIAL

2-18. Fisher, Experimental Shock Wave Reflection Studies with Several Different Reflecting Surfaces, NAVORD Report 2123, September 1951, UNCLASSIFIED

2-19. Hoffman and Mills, Air Blast Measurements About Explosive Charges at Side-on and Normal Incidence, BRL-988, July 1956, UNCLASSIFIED

4.4.2.2 Penetration. When a jet strikes a target of mild steel or armor plate, pressures of the order of 250,000 atmospheres are generated at the point of contact. Since this is far above the yield strength of any steel the target flows out of the path of the jet as would a fluid. There is so much radial momentum associated with the flow that the diameter of the hole produced is much larger than that of the jet. The difference in diameter between the jet and the hole it produces is not constant; that is, it depends upon the characteristics of the target material. For instance, a hole of much larger diameter is found in mild steel than in homogeneous armor plate. However, the depth of penetration of a jet into very thick slabs of mild steel or armor plate is nearly equal.

The kinetic energy from the particles is dispersed radially as the particles strike the target (Figure 4-[illegible]). Primary penetration is complete when the last jet particle strikes the target. The actual penetration does not stop until the kinetic energy imparted to the target material by the jet is dissipated. The slight additional penetration caused by this afterflow is known as secondary penetration. The depth of secondary penetration depends upon target strength. It is believed that this accounts for the slight difference in the depth of penetration in mild steel and in armor plate. The probability of some differences in the depth of primary penetration into these two metals must not be overlooked either.

The steady-state penetration, equation (4-13),

$$P = l\left(\frac{\lambda\rho_j}{\rho_t}\right)^{\frac{1}{2}} \tag{4-13}$$

which holds only for idealized jets whose properties remain constant throughout the penetration process, had to be modified to take into consideration jets that are not constant but which change character as they travel[4-1]. In equation (4-13), $\lambda$ equals a factor which accounts for the nature of the jet (particulate or fluid), $l$ equals the length of the jet and $\rho_j$ and $\rho_t$ the densities of the jet and target material respectively.

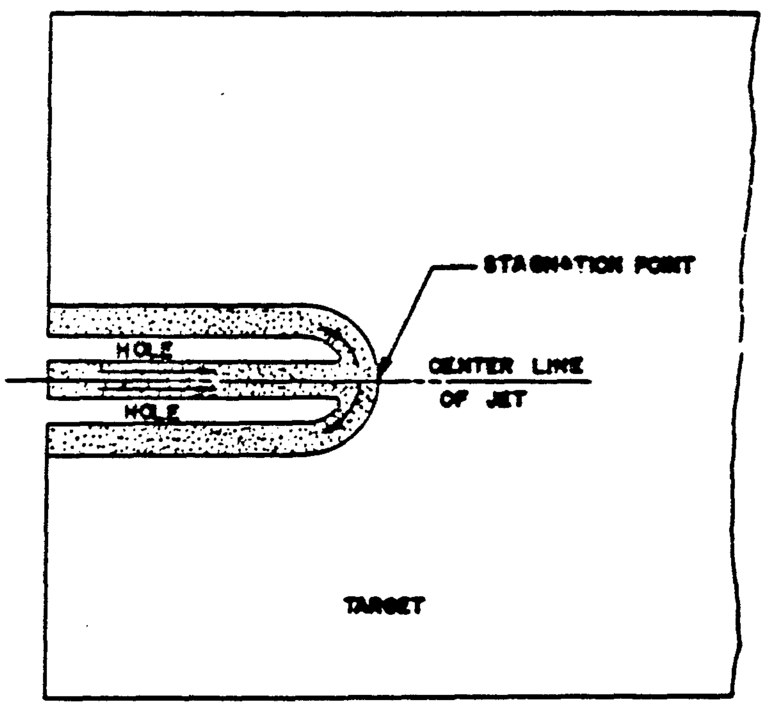


FIGURE 4-11 TARGET PENETRATION

Pugh[4-2] took into account the velocity distribution in the jet, and the variation of $V_j$ with penetration distance. Pugh's[4-1] equation for penetration is

$$P = \int U_p \, dt = \rho_t^{-\frac{1}{2}} \int (\lambda \rho_j)^{\frac{1}{2}} \, d\ell = \bar{J} \rho_t^{-\frac{1}{2}} \bar{\ell} \qquad (4\text{-}14)$$

where $\bar{J}$ and $\bar{\ell}$ are average quantities taking into account the variation of $\lambda \rho_j$ and $\ell$ in time for the element of the jet effective in penetrating the target at time t.

The penetration equation presented by Eichelberger[4-7] is

$$P = \ell \sqrt{\frac{\gamma \rho_\ell}{\rho_t} - \frac{\sigma}{\frac{1}{2} \rho_t (V_j - U_p)^2}} \qquad (4\text{-}15)$$

where $V_j$ and the penetration velocity $U_p$ are instantaneous values, $\gamma \rho_\ell$ is substituted for $\lambda \rho_j$, and $\sigma$ equals the difference between $\sigma_t$ (target hardness) and $\sigma_j$ (jet hardness). $\gamma$ is a statistical factor which depends on all of the factors that produce changes in either $\lambda$ or $\rho_j$.

## 4.5 PENETRATION FACTORS

Many factors affect shaped charge performance; some of them will be discussed in the following sections.

### 4.5.1 RATE OF DETONATION, TYPE AND DENSITY OF EXPLOSIVE CHARGE.

For standard conditions a difference in the depth of penetration and in cavity volume is readily seen when different explosive loadings are used. Table 4-1 is a tabulation of explosive performance observed in static penetration tests at the NOL/WO. Testing was performed with cylindrical charges. The geometry of the charges tested was standardized; that is, the charges had a diameter of 1.63 inches, were 4.0 inches high, were cast or pressed over M9A1 type steel conical liners, were point initiated, and were fired into mild steel targets at a standoff distance of 4.0 inches.

The octol group (HMX/TNT) of explosives offers up to 20 percent greater penetration than the other explosives tested and satisfy such requirements as sensitivity, availability, compatibility, etc., but with the possible exception of cost[4-4b]. Burke, Cook, and others at duPont showed that with a knowledge of the density and detonation velocity of an explosive a good estimate of performance might be obtained[4-8]. More specifically, results from tests performed with steel, aluminum, and copper liners revealed that both depth of penetration and cavity volume were a linear function of the detonation pressure. Figure 4-12 shows the variation of penetration with detonation pressure for a number of the explosives given in Table 4-1. Figure 4-13 is somewhat similar to Figure 4-12 with the exception that three different types of liner materials were used.

TABLE 4-1 SHAPED CHARGE PENETRATION WITH VARIOUS EXPLOSIVES[4-4b]

| Explosive | Density (gm/cc) | Detonation Vel. (m/sec) | Penetration (in.) |
|---|---|---|---|
| 77/23 HMX/TNT | 1.80 | 8490 | 7.45 |
| 75/25 HMX/TNT | 1.80 | 8430 | 7.39 |
| PTX-2 | 1.68 | 8000 | 6.57 |
| 75/25 RDX/TNT | 1.68 | 8060 | 6.24 |
| 70/30 RDX/TNT | 1.69 | 7930 | 6.21 |
| 60/40 RDX/TNT | 1.68 | 7850 | 6.17 |
| 91/9 RDX/Wax | 1.61 | 8340 | 6.06 |
| 90/10 BTNEN/Wax | 1.70 | 8130 | 5.65 |
| 50/50 Pentolite | 1.65 | 7600 | 5.53 |
| PBX | 1.61 | 7980 | 5.17 |
| HBX-1 | 1.[illegible]9 | 7440 | 5.16 |
| 70/30 Tetryl/TNT | 1.63 | 7370 | 5.13 |
| H-6 | 1.73 | 7460 | 4.52 |
| TNT | 1.60 | 6980 | 4.25 |
| 91/9 RDX/Wax | 1.30 | 7000 | 4.20 |

4.5.2 WARHEAD CASING DESIGN. The warhead casing has a dual purpose. It must retain the explosive prior to detonation and confine the charge during detonation. This confinement effect is noted whether the confinement is provided by an increase in wall thickness or by a "belt" of explosive. A result of increasing the confinement is an increase in hole volume in the target material.

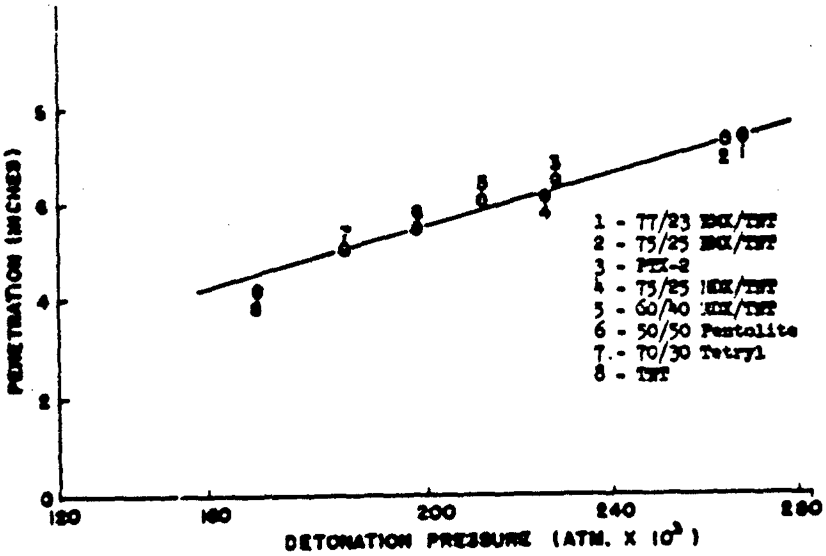


FIGURE 4-12 PENETRATION VS DETONATION PRESSURE FOR VARIOUS EXPLOSIVES[4-40]

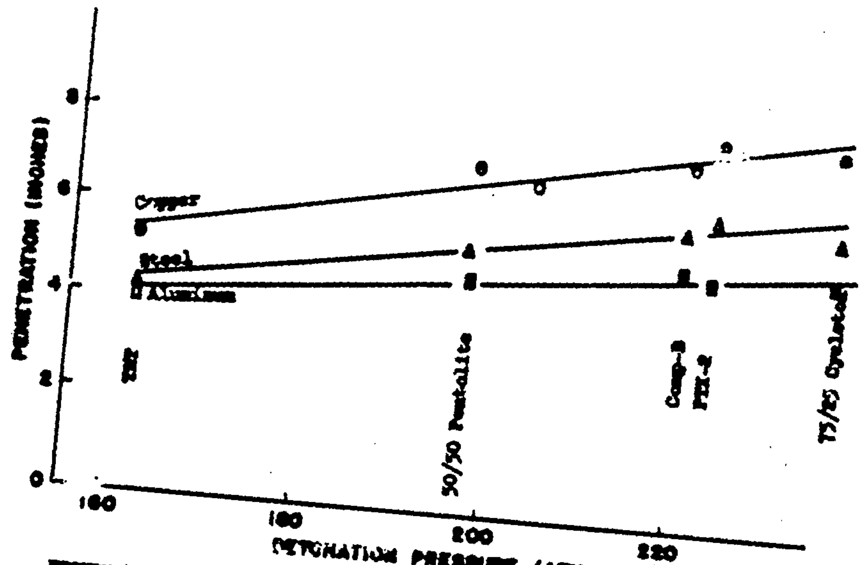


FIGURE 4-13 PENETRATION VS DETONATION PRESSURE FOR VARIOUS LINER MATERIALS[4-4b]

In effect, it decreases the loss of pressure laterally and increases the duration of the application of pressure. Going a little further, it is important to note that the strength of the case required for confinement during detonation is practically nil for warheads with charge length to diameter (L/D) ratios which exceed approximately 4. As the L/D of the charge is reduced the case strength required for confinement increases. In guided missile applications, the case thickness for optimum confinement is not usually obtained because of weight limitations.

4.5.3 SHAPE OF CHARGE BACK OF LINER. Aerodynamic performance and projectile weight specifications are factors that frequently limit the length of the projectile body, which in turn, limits the length of the charge. Generally speaking, the hole volume and the penetration obtained increase with increasing charge length and reach a maximum at about 2 or 2.5 charge diameters for heavily confined charges or 4 charge diameters for lightly confined or unconfined charges. There are many shaped charge designs but the ones most frequently used are illustrated in Figure 4-14. Each design has its advantages: configuration (a) has the advantages of ease in manufacture, high explosive loading, and blast effect; (b) and (c) are sometimes necessitated by the requirements for accuracy, weight and space limitations. All three designs can be made to perform satisfactorily. The greater amount of explosive in the cylindrical charge makes it more valuable than the tapered charges for the secondary effects of blast and fragmentation.

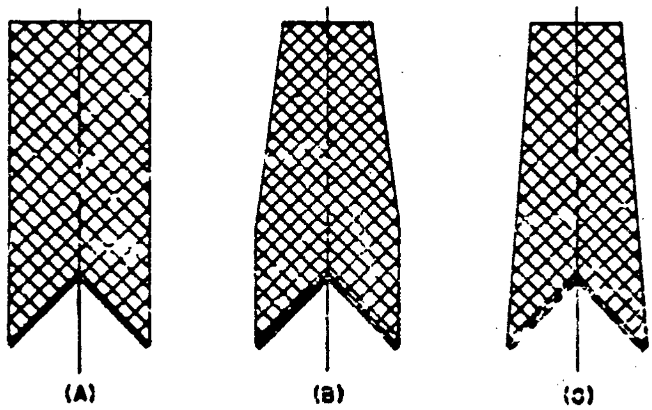


FIGURE 4-14 TYPICAL SHAPED CHARGE BODY DESIGNS

4.5.4 LINER VARIATIONS. Warping of as little as 1/32" on two sides of a cut down steel M9A1 cone (base diminished from 1-5/8" to 1" I.D.) caused by dropping or other mishandlings is sufficient to lower jet penetration by 1.24 charge diameters[4-12]. Cones used in tests outlined in reference 4-12 having .015", .025", .037" and .050" wall thickness are extremely susceptible to damage from rough handling, especially the cones with wall thicknesses of .015" and .025". Warped cones, as previously mentioned, which are produced during the drawing process or by damage from rough handling give very poor penetration. Further, as noted in reference 4-12, it has been found that a bead of weld on the inside cone surface, running from the apex to base of the cone, lowers penetration one cone diameter from a standard penetration average of 3.7 cone diameters, whereas a similar bead on the outside surface lowers penetration by 0.08 cone diameters.

4.5.5 LINER MATERIAL, THICKNESS AND MASS. Rather than use less dense material for liners an efficient way to reduce liner weight would be to design a more efficient charge configuration. The metals most used in liners are aluminum, steel, and copper. By using a liner material of high density or by increasing the liner thickness it is possible to increase the jet mass per unit length. By decreasing the mass per unit area of the liner it is possible to increase the jet velocity.

The conditions for maximum destructiveness and those for maximum penetration are incompatible. The designer must seek the most satisfactory compromise. When low density materials are used for liners the destructiveness attained is maximized but at the expense of the depth of penetration. As of 1958 the only low density material which performed satisfactorily was aluminum[4-13]. Two ways to make up for the reduction of penetration resulting from the use of low density aluminum, are (a) peripheral initiation and (b) double angle liners.

Liners of high density metals tend to maximize the penetration depth at the expense of destructiveness, but if maximum destruction is required without regard to penetration, it can be accomplished by reducing the penetration to a point where defeat of the target is assured. This, at present, is the easier approach.

Curves showing penetration vs wall thickness are frequently unsymmetrical. Figure 4-15 illustrates penetration with various wall thicknesses. Dimensions pertaining to the shaped charge tested can be found in reference 4-13.

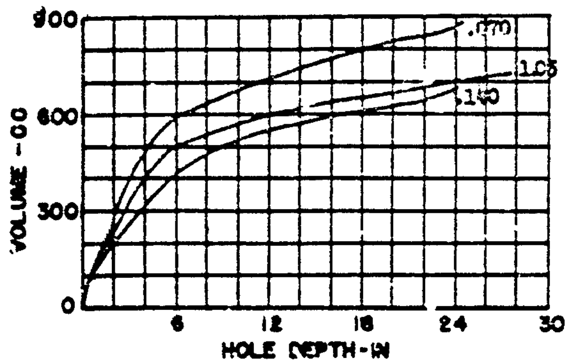


CUMULATIVE VOLUME VS HOLE DEPTH

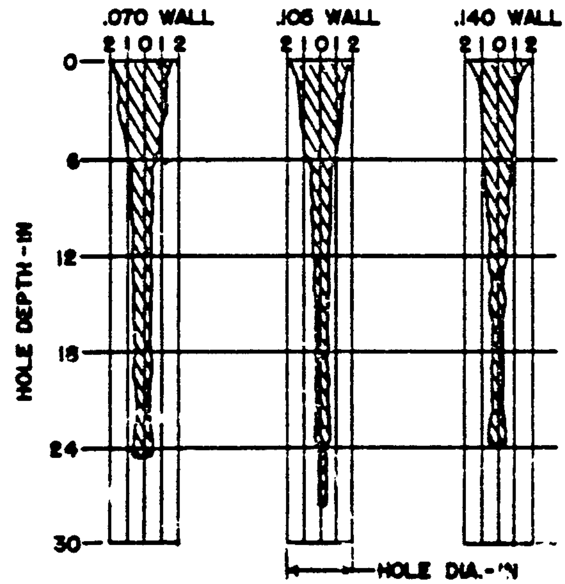


HOLE DIAMETER VS HOLE DEPTH

FIGURE 4-25 CUMULATIVE VOLUME CURVES AND PROFILES OF PENETRATION AT 11 INCHES STANDOFF

Conical liners with tapered walls have been studied at various times. In general, the results indicate that no significant improvement of penetration performance can be achieved by use of a tapered wall thickness[4-4c]. The data do show, however, that rather wide tolerances may be placed on the variation in wall thickness between the apex and the base without reducing penetration, provided the wall thickness is held constant at each transverse section of the cone.

Cone thickness, for best performance, is primarily a function of cone apex angle and charge confinement, but other parameters play lesser roles. Optimum liner wall thickness increases with increasing cone angle and with increasing confinement of the explosive charge. Generally, the optimum liner wall thickness varies between 2 and 4 percent of the base diameter. Work has been done using cone thicknesses as high as 18 percent of the base diameter. Thicknesses of approximately 6 percent are generally used in warheads that are fired against aircraft at long standoffs.

Liner walls thicker than optimum show a slight decrease in penetration. Liner walls thinner than optimum are characterized by inconsistent penetration and an overall decrease in penetration[4-15]. Penetration will increase to a maximum as the liner thickness is decreased, at which point the manufacturing imperfections become more important and further decrease of the liner thickness results in less penetration.

4.5.6 WAVE SHAPING. Wave shaping is a method of improving shaped charge performance. Its purpose is to invert the detonation wave and cause it to strike the cone wall at decreased angles of obliquity. Wave shapers are placed between the detonator and liner. The base of the wave shaper is generally located immediately behind the apex of the cone. Wave shaping can be accomplished by inert fillers, voids in the explosive charge, or other explosive fillers.

Solid cone-shaped inert fillers of glass or steel have produced 20 percent deeper penetrations without loss of hole volume[4-15]. It was found that cone-shaped inert fillers, with a base-to-altitude ratio of two, perform well with small reduction in performance for slightly different ratios. The diameter of the wave shaper is slightly less than that of the charge. Wave shapers can be designed so that the detonation wave passes directly through the filler which produces wave refraction, and thus the end result is a considerable improvement in penetration without loss in the hole volume.

Peripheral initiation is another method of wave shaping, however, the actual improvement attained is affected considerably by the liner material used. Hole volume has been increased as much as 50 percent[4-15]. Small asymmetries anywhere in the charge will decrease penetration. Results from peripheral initiation are not consistent; therefore, some other method of initiation should be used. More consistent results can be obtained with point-initiated charges and, in addition, this type charge is easier to manufacture. Figure 4-16 illustrates a number of different wave shaping configurations.

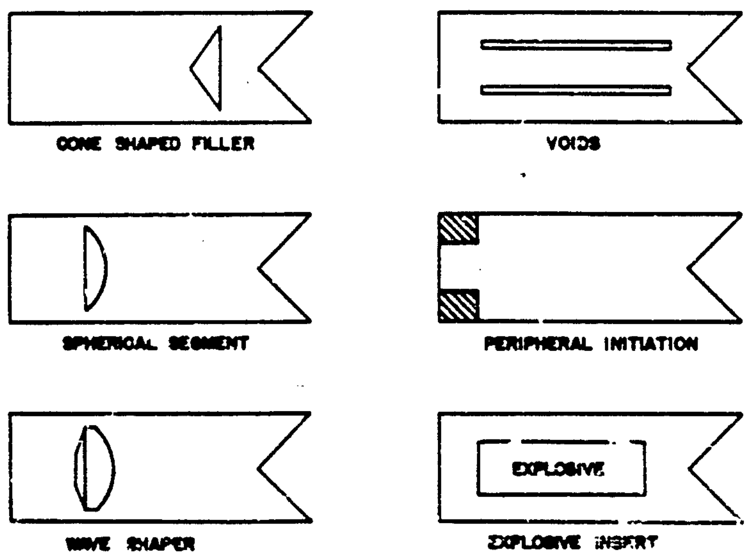


FIGURE 4-16 EXPLOSIVE CHARGE WAVE SHAPERS

4.5.7 CONE APEX ANGLE. Cone apex angles play a very important role in shaped charge performance. When selecting a cone angle for a shaped charge it is important to consider both performance and manufacturing problems involved. There are data available which show optimum standoff increases with increasing cone apex angles up to approximately 65°; optimum standoff then decreases as the apex angle is increased. (See Figures 4-17 through 4-20.) However, the optimum standoff is also dependent upon the cone material, wall thickness, and charge length[4-5].

Cone apex angles from 40 to 60 degrees give good performance at the standoff usually associated with surface targets; that is, two to four cone diameters. Increased penetration can be achieved with good quality cones, utilizing smaller cone angles of 20 to 30 degrees, at standoffs below approximately two cone diameters. This is particularly true with copper liners (see Figure 4-17). Performance from cones with smaller apex angles give only moderate improvement in performance[4-15]. This small advantage in performance would usually be outweighed by the tightening of manufacturing tolerances. There are ample experimental data which show improved penetration at long standoffs, for cones with apex angles of 80 to 120 degrees or more[4-15]. Cones with apex angles of 80° to 120° are recommended for use against aircraft at standoff distances on the order of 100 feet[4-15].

4.5.8 LINER SHAPE. Liners and cavities of different configurations react in different ways. For example, hemispherical liners appear to turn inside out with most of the cone material being projected in the jet. On the other hand a conical liner collapses from the apex and projects approximately 20 to 30 percent of the cone material in the jet. Most work is done with conical liners because they give the most consistent results. This is true because it has been more difficult to maintain close tolerances with shapes other than conical. Double angle conical liners are being studied[4-13]. Figure 4-21 shows a double angle liner where the upper and lower portions are conical and are connected by a circular fairing curve. Penetration for this type liner, at the two standoffs tested[4-13], compare favorably with the maxima of peripheral initiation. When double angle cones were being developed it was found that there is no increase in penetration when an abrupt change is made from one angle to another.

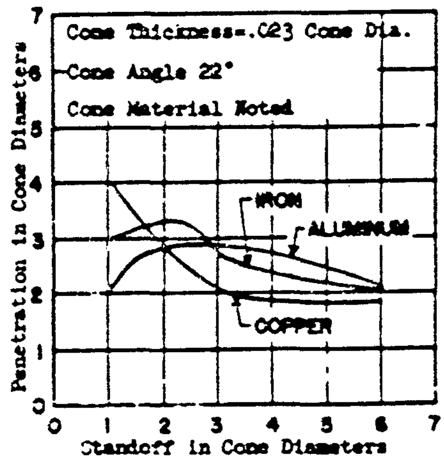


FIGURE 4-17 PENETRATION VS STANDOFF AGAINST MILD STEEL TARGETS

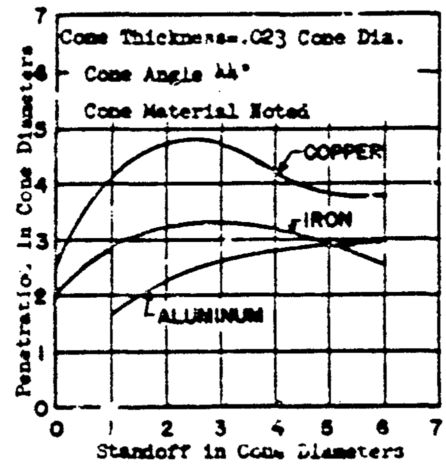


FIGURE 4-18 PENETRATION VS STANDOFF AGAINST MILD STEEL TARGETS

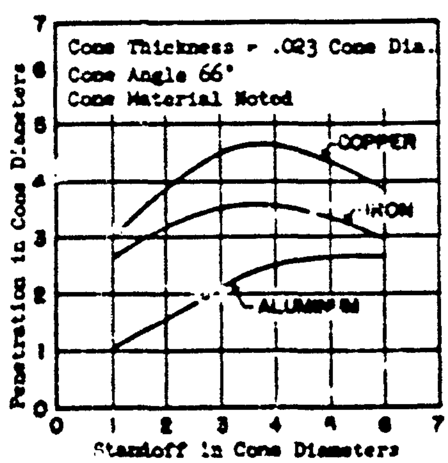


FIGURE 4-19 PENETRATION VS STANDOFF AGAINST MILD STEEL TARGETS

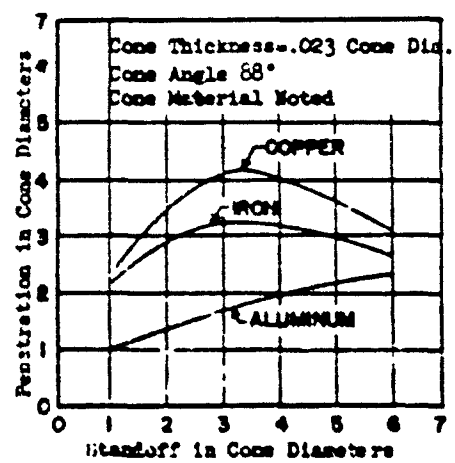


FIGURE 4-20 PENETRATION VS STANDOFF AGAINST MILD STEEL TARGETS

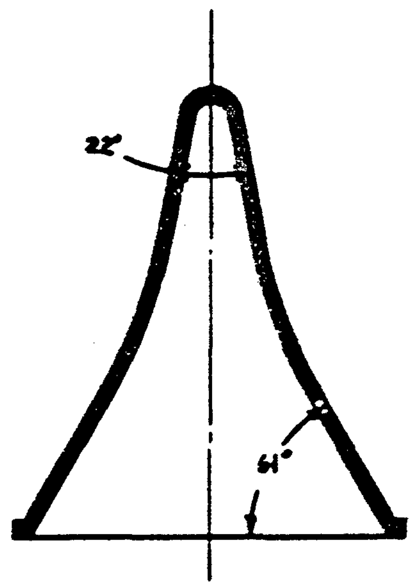


FIGURE 4-21 TYPICAL DOUBLE ANGLE LINER DESIGN USED. UPPER AND LOWER PORTIONS ARE CONICAL AND ARE CONNECTED BY A CIRCULAR FAIRING CURVE.[4-13]

4.5.9. EFFECT OF SPIT-BACK (FLASH BACK) TUBES. The spit-back tube, used with certain types of fuzing, is a small tube that is attached to the apex end of the cone, extending away from the cavity. The portion of the liner apex inside the spit-back tube is removed. Results from tests with unconfined M3A1 cones show little change in penetration or a slight decrease. Data from tests with copper liners in confined charges with spit-back tubes show increases in penetration up to 20 percent[4-15]. There is no effect upon optimum standoff or optimum wall thickness. It is easier to manufacture cones with a short spit-back tube and to maintain close tolerances than it is to manufacture cones with a sharp cone apex angle. In addition, less difficulty is encountered in obtaining sound charges when spit-back tubes are used.

Satisfactory performance can be obtained with tubes having a diameter between 20 to 30 percent of that of the cone. It is common procedure to specify hard-drawn copper tubing with wall thickness ranging from 0.060 to 0.065 inches for spit-back tubes[4-5].

4.5.10 ALIGNMENT OF CONE AND CHARGE. For best performance the axis of the cone and explosive charge should coincide. Tilt of a liner results in reduced penetration. Tilts up to two degrees have given some good penetrations, but in general tilting the liner one degree reduces average penetration 50 percent[4-5]. Misalignment of the cone and charge axes, where the axes are parallel but offset, results in reduced penetration. In a particular instance, an offset of only 0.015 inch (1 percent of the base diameter) reduced the penetration about 20 percent[4-5]. Because of the poor results obtained from tilt and offset of axes it is important that charges be inspected after assembly.

4.5.11 STANDOFF DISTANCE. Standoff distance is one of the most important factors governing the depth of penetration for a given shaped charge warhead. A properly designed warhead must provide correct standoff distance to allow sufficient time for the fuze to function properly and the formation of a jet of proper density, thus maximizing the possibility of target penetration. The dependence of penetration depth upon standoff is shown in Figures 4-17 through 4-20.

## 4.6 SCALED SHAPED CHARGES

The Ballistic Research Laboratories[4-16] investigated jets produced from three conical copper liners, scaled in all linear dimensions, having an apex angle of 42 degrees. The dimensions of the scaled charges investigated are presented in Figure 4-22. The BRL study was carried on to determine the effect of charge size upon jet flight and jet penetration characteristics. Effective penetration by a jet ceases when the particle velocity drops slightly below 0.2 cm/microsecond[4-17]. Based on this criterion BRL did not take measurements of jet particles below this lower velocity limit.

Results from these tests, with the three charges just mentioned, show that scaled shaped charges produce scaled penetration depths at scaled standoff distances. Jet velocities, penetration velocities and relative penetration depths are the same at scaled times during the penetration process. In addition, radiographic observation disclosed that jets from scaled conical liners in scaled charges produce approximately the same number of particles after breakup is completed. These tests revealed that the average particle length scales directly as the charge size and that the average particle diameter varies directly as the charge size so that the average particle volume and mass vary as the cube of the charge size[4-18].

Figures 4-23 through 4-25 illustrate part of the experimental results of testing performed with the three scaled copper conical liners mentioned under this section. In these figures x represents the distance from the inside cone apex to a particular circumferential ring element on the inside liner surface; h the total cone height; t a particular time; D cone diameter. Standoff distance for these tests was three cone diameters.

## 4.7 REFERENCES FOR SECTION 4

4-1. M. A. Cook, The Science of High Explosives, Reinhold Publishing Corporation, 1958
4-2. G. Birkhoff, D. P. MacDougall, E. M. Pugh, and Sir G. Taylor, "Explosives with Lined Cavities," Journal Applied Physics 19, 1948, 563-582
4-3. R. J. Eichelberger and E. M. Pugh, "Experimental Verification of the Theory of Jet Formation by Charges with Lined Conical Cavities," Journal of Applied Physics 23, 1952, 537-542
4-4. Transactions of Symposium on Shaped Charges, Ballistic Research Laboratories Report No. 909, 1953, CONFIDENTIAL
(a) J. Simon and L. Zernow, "High Strain Rate Plasticity of Liner Materials and Jet Behavior," 107-130 CONFIDENTIAL

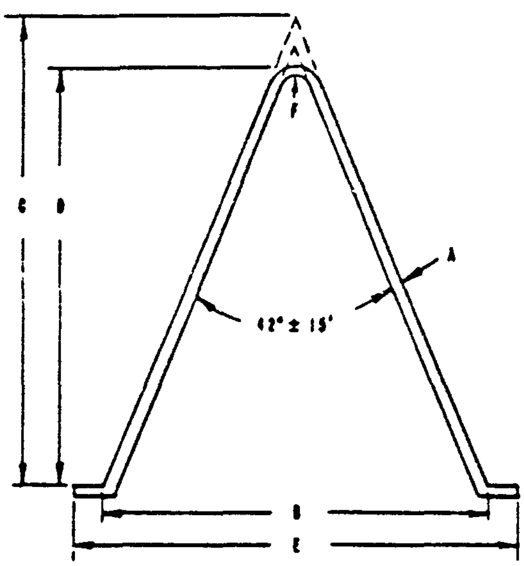


| | | SCALE SIZE NO. | | |
|---|---|---|---|---|
| | DIMENSIONS | 2 | 3 | 4 |
| A | NOMINAL WALL THICKNESS ⊥ WALL (IN.) | 070 | 0.105 | 0.140 |
| B | CONE DIAMETER (INCHES) | 1.890 | 2.835 | 3.780 |
| C | THEORETICAL ALTITUDE (INCHES) | 2.4618 | [illegible].6927 | 4.[illegible]238 |
| D | GEOMETRICAL HEIGHT (INCHES) | 2.238 | 3.357 | 4.478 |
| E | FLANGE DIAMETER (INCHES) | 2.050 | 3.075 | 4.100 |
| F | INSIDE RADIUS (INCHES) | 0825 | .083 | 0.12[illegible] |
| | MEASURED CONE MASS (GMS.) | 82.53 | 278.8 | 892.9 |

FIGURE 4-22

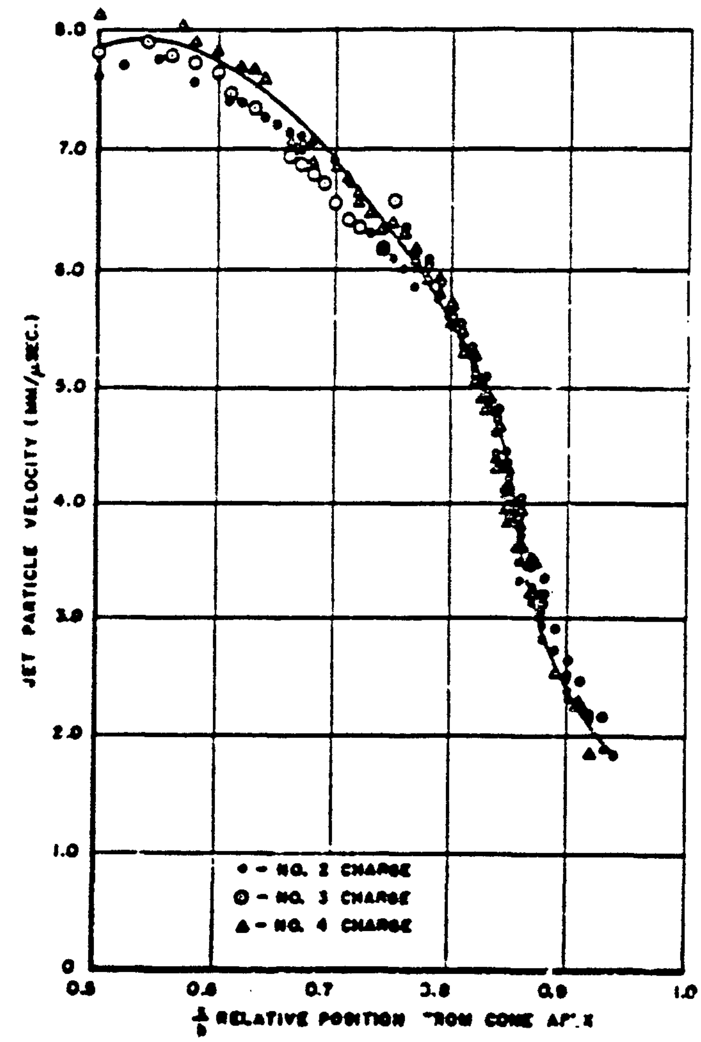

8.0
7.0
6.0
5.0
4.0
3.0
2.0
1.0
0
0.5
0.6
0.7
0.8
0.9
1.0
JET PARTICLE VELOCITY (MM/μSEC.)
RELATIVE POSITION FROM CONE APEX
• – NO. 2 CHARGE
○ – NO. 3 CHARGE
▲ – NO. 4 CHARGE


FIGURE 4-2

(b) W. T. August and A. D. Solem, "Shaped Charge Effects Attributable to the Explosive Components," 180-191, CONFIDENTIAL

(c) H. Winn, "The Present Status of the Artillery, Ammunition Program at the Firestone Tire and Rubber Company," 15-42, CONFIDENTIAL

4-5. Section, Design for Terminal Effects, Ordnance Corps Pamphlet ORDP 20-245 May 1957, CONFIDENTIAL

4-6. R. J. Eichelberger, "Re-Examination of the Nonsteady Theory of Jet Formation by Lined Cavity Charges," Journal Applied Physics, 26, 1955 398-402

4-7. R. J. Eichelberger, "Experimental Test of the Theory of Penetration by Metallic Jets," Journal Applied Physics 27, 1956, 63-68

4-8. W. R. Burk, Investigation of Cavity Effects Section III Variation of Cavity Effect with Explosive Composition, E. I. duPont de Nemours & Co., 3 Feb 1953

4-9. R. J. Eichelberger, "Survey of Present Status of Shaped Charge Research," Transactions of Symposium on Shaped Charges, Ballistic Research Laboratories Report No. 985, 1956, 1-5, CONFIDENTIAL

4-10. D. E. Laskowski and W. C. McCrone, Casting of TNT, Final Report by Armour Research Foundation of Illinois Institute of Technology, 25 June 1952

4-11. I. Liberman and A. Merendino, A Comparison of Explosive Loading Techniques Upon Shaped Charge Penetration, Ballistic Research Laboratories Report No. 964, January 1956, CONFIDENTIAL

4-12. J. Panyarella and J. Longobardi, Performance of Shaped Charges with Intentionally Deformed Liners, Ballistic Research Laboratories Report No. 811, March 1952, CONFIDENTIAL

4-13. R. J. Eichelberger, et al, A Critique on the Design of the T-42 Warhead, Ballistic Research Laboratories Report No. 1212, June 1958, CONFIDENTIAL

4-14. E. M. Pugh, R. J. Eichelberger, and N. Rostaker, "Theory of Jet Formation by Charges with Lined Conical Cavities," Journal Applied Physics, 23, 1952, 532-536

4-15. Warheads General Ordnance Corps Pamphlet, ORDP 20-290, July 1959, CONFIDENTIAL

4-16. R. Di Persio, J. Simon, and T. H. Martin, A Study of Jets from Scaled Conical Liners, Ballistic Research Laboratories Report No. 1298, 1960, CONFIDENTIAL

4-17. R. Di Persio, J. Simon, An Empirical Approach to the Design of a Spin-Compensating Shaping Charge Liner, Ballistic Research Laboratories Report No. 1251, February 1960, CONFIDENTIAL

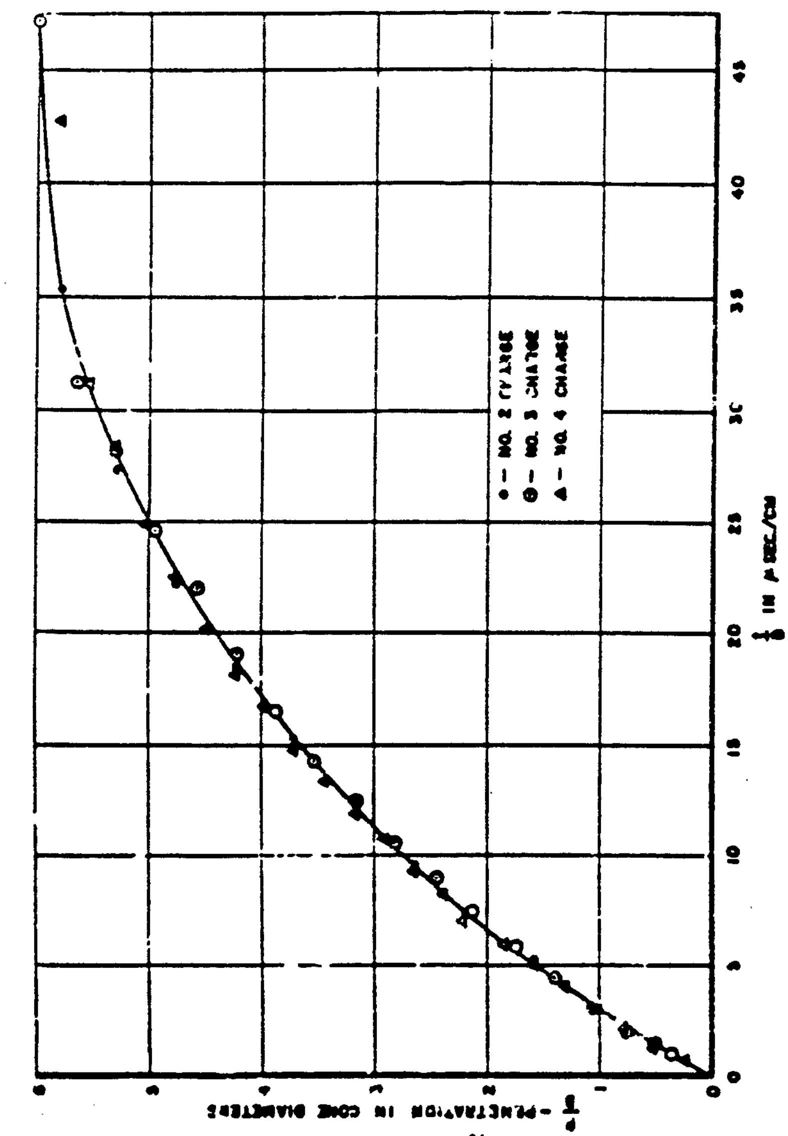
0
1
2
3
4
5
6
$\frac{P}{D}$ - PENETRATION IN CONE DIAMETERS
0
5
10
15
20
25
30
35
40
45
$\frac{1}{V}$ IN μ SEC./CM
• — NO. 2 CHARGE
⊙ — NO. 3 CHARGE
▲ — NO. 4 CHARGE

FIGURE 4-24

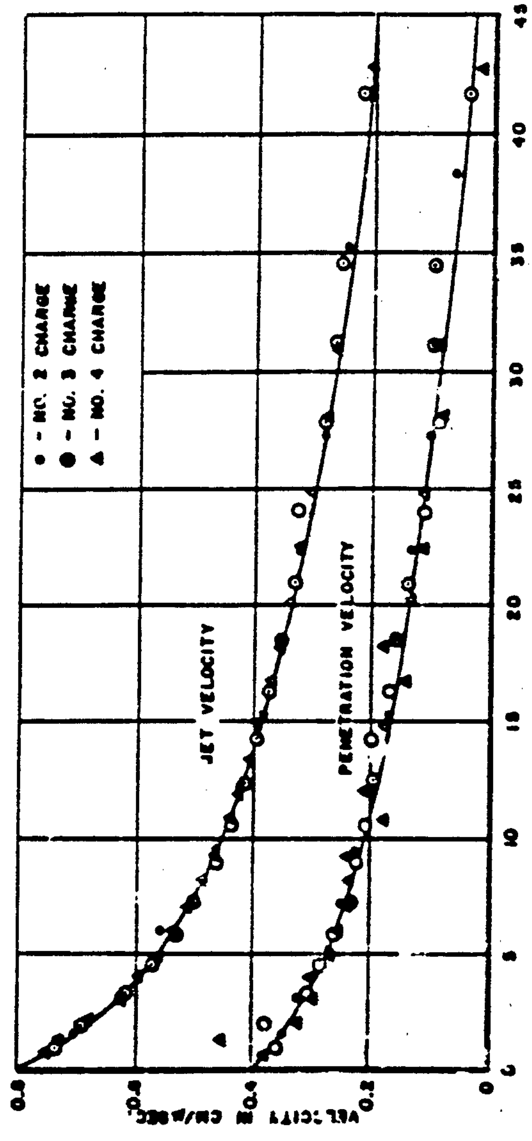

• - NO. 2 CHARGE
● - NO. 3 CHARGE
▲ - NO. 4 CHARGE
JET VELOCITY
PENETRATION VELOCITY
VELOCITY IN CM/μSEC.
0
0.2
0.4
0.6
0.8
0
5
10
15
20
25
30
35
40
45
1/b IN μSEC./CM


FIGURE 4-[illegible]

## DISTRIBUTION

| | |
|---|---|
| Bureau of Naval Weapons | |
| DLI-31 | 1 |
| RMMO | 2 |
| RMMO-4 | 1 |
| RMMO-422 | 2 |
| RMMO-5 | 2 |
| RMMO-52 | 1 |
| RM | 1 |
| RMMO-13 | 1 |
| RM-24 (LTCOL Patton, USMC) | 2 |
| Defense Documentation Center<br>Cameron Station<br>Alexandria, Virginia | 20 |
| Commanding General<br>Aberdeen Proving Ground<br>Aberdeen, Maryland<br>Attn: Technical Information Section<br>Development and Proof Services | 2 |
| Commander, Test and Evaluation Force<br>Norfolk 11, Virginia | 1 |
| Ballistics Research Laboratories<br>Aberdeen, Maryland<br>Attn: Mr. D. J. Dunn, Jr. | 1 |
| Attn: Dr. Fichelberger | 1 |
| Commander<br>Naval Ordnance Test Station<br>China Lake, California | 2 |
| Commander<br>Naval Ordnance Laboratory<br>White Oak, Silver Spring, Maryland | 1 |
| Attn: Mr. Solem | 1 |
| Commanding Officer<br>Picatinny Arsenal<br>Dover, New Jersey | 1 |

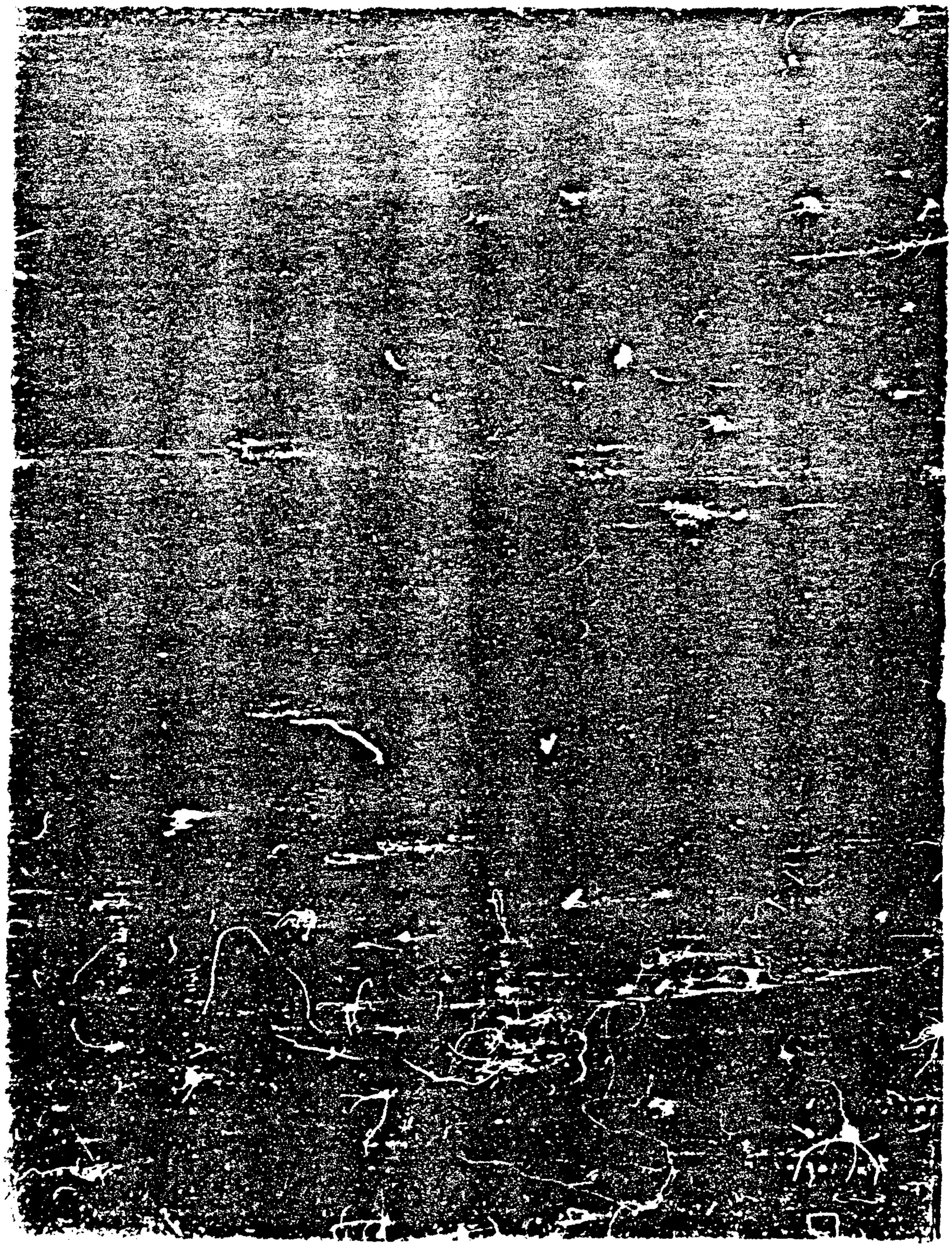

DISTRIBUTION (Continued)

| | |
|---|---|
| Commanding General<br>Patrick AFB, Florida<br>Attn: COL L. T. Geyer | 1 |
| Director<br>Naval Research Laboratory<br>Washington 20, D. C. | 1 |
| Chief of Ordnance<br>Department of the Army<br>Washington 25, D. C. | 1 |
| Applied Physics Laboratory<br>Johns Hopkins University<br>Silver Spring, Maryland<br>Attn: Mr. R. Larsen<br>Via: BUWEPS | 1 |
| Commander<br>David Taylor Model Basin<br>Washington, D. C.<br>Attn: F. Weinberger | 1 |
| Bureau of Ships<br>Washington, D. C.<br>Attn: K. Lobell | 1 |
| Engineering Library, Plant 5<br>Grumman Aircraft Engineering Corp.<br>Bethpage, Long Island, New York | 1 |
| Commanding Officer<br>U. S. Naval Ordnance Laboratory<br>Corona, California | 1 |
| Northwestern University<br>Aerial Measurements Lab.<br>2422 Oakton Street<br>Evanston, Illinois | 1 |
| Hq. Tactical Air Command<br>Langley Air Force Base, Virginia<br>Attn: Operations Analysis | 3 |

DISTRIBUTION (Continued)

| | |
|---|---|
| Commanding Officer<br>Watertown Arsenal<br>Watertown, Massachusetts | 1 |
| Commanding Officer<br>Frankford Arsenal<br>Bridge and Tacony Streets<br>Philadelphia, Pennsylvania | 1 |
| Commander<br>Air Proving Ground Center<br>Air Research and Development Command<br>Eglin Air Force Base, Florida | |
| Attn: APGC (PGAPI) | 2 |
| Attn: APGC (PGWR) | 1 |
| Attn: Contract AF 08(635)-3522, PGXX | 1 |
| Minneapolis Honeywell Regulator Co.<br>Ordnance Division<br>Hopkins, Minnesota | 1 |
| General Dynamics<br>Box 1011 Mail Zone 6-51<br>Pomona, California<br>Attn: C. L. McMillan | 1 |
| Commanding Officer<br>Picatinny Arsenal<br>Dover, New Jersey SMUPA-VA-6<br>Attn: Technical Information Section | 1 |
| Chief of Naval Operations<br>Pentagon Building<br>Washington, D. C.<br>Attn: William Okeef (OP03EG) | 5 |
| Weapon Systems Evaluation Group<br>Pentagon Building<br>Washington 25, D. C. | 1 |
| Commanding Officer<br>U. S. Naval Propellant Plant<br>Indian Head, Maryland<br>Attn: NAVEODFAC/PUL:RBT | 1 |

DISTRIBUTION (Continued)

| | |
|---|---|
| Sandia Corporation<br>Sandia Base, Albuquerque, New Mexico<br>Attn: R. L. Calvert - Code 5422 | 1 |

Standard Navy Distribution List,
Part I Numbers as Follows:

21
22
24
24B
24C (Less COMCRUDESPACLOGREP, Long Beach)
24J

Local:

| | |
|---|---|
| T | 1 |
| TD | 1 |
| TDP | 5 |
| TR | 1 |
| TE | 1 |
| TEV-3 | 1 |
| WX | 1 |
| KRT | 1 |
| TE-2 | 1 |
| TEE | 1 |
| TY | 1 |
| KXB | 2 |
| KXH (A. V. Hershey) | 1 |
| ACL | 5 |
| File | 1 |

DISTRIBUTION (Continued)

| | |
|---|---|
| Naval Weapons Services Office (Code 120)<br>Naval Weapons Plant<br>Washington 25 D. C. | 7 |
| Chief of Naval Operations<br>Washington 25, D. C.<br>Attn: OP-725 | 2 |
| Bureau of Naval Weapons<br>Fleet Readiness Representative, Pacific<br>Naval Air Station, North Island<br>San Diego 35, California | 1 |
| CAPT O. L. Dawson, Jr.<br>Hq. USAF (AFCIN-3K2)<br>Washington 25, D. C. | 1 |
| Mr. M. H. Keith (Code 4034)<br>NOTS<br>China Lake, California | 1 |
| The Martin Company<br>Orlando, Florida | 1 |
| NMC<br>Pt. Mugu, California<br>Attn: Mr. C. Campbell | 1 |
| Department of Defense<br>Defense Intelligence Agency<br>DIAAP-1K2<br>Washington, D. C.<br>Attn: S. E. Whitney<br>Attn: A. W. Holt | <br><br><br><br>1<br>1 |
| Bureau of Naval Weapons<br>Munitions Bldg.<br>Room 2009<br>Attn: DSC-31 | 1 |
| COMOPTEVFOR | 1 |
| DEPCOMOPTEVFORPAC | 1 |
| VX-5 | 1 |

Naval Weapons Laboratory (NAVWEPS Report No. 7673)
PRELIMINARY WARHEAD TERMINAL BALLISTIC HANDBOOK. PART 1: TERMINAL BALLISTIC EFFECTS (U), by C. Johnson and J. W. Moseley. 31 March 1964. 98 p., 53 figs., 6 tables. (NWL Report No. 1821)

CONFIDENTIAL

This report is contained in two separate parts.
Part 1, Terminal Ballistic Effects, presents a summary of the laws, parameters and equations associated with conventional kill mechanisms.

1. Terminal ballistics - Handbooks
2. Weapons - Terminal ballistics
I. Johnson, C.
II. Moseley, J. W.
III. NAVWEPS 7673
IV. Title: Warhead Terminal Ballistic Handbook

Abstract card is UNCLASSIFIED

Naval Weapons Laboratory (NAVWEPS Report No. 7673)
PRELIMINARY WARHEAD TERMINAL BALLISTIC HANDBOOK. PART 1: TERMINAL BALLISTIC EFFECTS (U), by C. Johnson and J. W. Moseley. 31 March 1964. 98 p., 53 figs., 6 tables. (NWL Report No. 1821)

CONFIDENTIAL

This report is contained in two separate parts.
Part 1, Terminal Ballistic Effects, presents a summary of the laws, parameters and equations associated with conventional kill mechanisms.

1. Terminal ballistics - Handbooks
2. Weapons - Terminal ballistics
I. Johnson, C.
II. Moseley, J. W.
III. NAVWEPS 7673
IV. Title: Warhead Terminal Ballistic Handbook

Abstract card is UNCLASSIFIED

Naval Weapons Laboratory (NAVWEPS Report No. 7673)
PRELIMINARY WARHEAD TERMINAL BALLISTIC HANDBOOK. PART 1: TERMINAL BALLISTIC EFFECTS (U), by C. Johnson and J. W. Moseley. 31 March 1964. 98 p., 53 figs., 6 tables. (NWL Report No. 1821)

CONFIDENTIAL

This report is contained in two separate parts.
Part 1, Terminal Ballistic Effects, presents a summary of the laws, parameters and equations associated with conventional kill mechanisms.

1. Terminal ballistics - Handbooks
2. Weapons - Terminal ballistics
I. Johnson, C.
II. Moseley, J. W.
III. NAVWEPS 7673
IV. Title: Warhead Terminal Ballistic Handbook

Abstract card is UNCLASSIFIED

Naval Weapons Laboratory (NAVWEPS Report No. 7673)
PRELIMINARY WARHEAD TERMINAL BALLISTIC HANDBOOK. PART 1: TERMINAL BALLISTIC EFFECTS (U), by C. Johnson and J. W. Moseley. 31 March 1964. 98 p., 53 figs., 6 tables. (NWL Report No. 1821)

CONFIDENTIAL

This report is contained in two separate parts.
Part 1, Terminal Ballistic Effects, presents a summary of the laws, parameters and equations associated with conventional kill mechanisms.

1. Terminal ballistics - Handbooks
2. Weapons - Terminal ballistics
I. Johnson, C.
II. Moseley, J. W.
III. NAVWEPS 7673
IV. Title: Warhead Terminal Ballistic Handbook

Abstract card is UNCLASSIFIED

LIBRARY CATALOGING INPUT

## BIBLIOGRAPHIC INFORMATION

| DESCRIPTOR | CODE | DESCRIPTOR | CODE |
|---|---|---|---|
| SOURCE Naval Weap.:s Laboratory | NPGA | SECURITY CLASSIFICATION AND CODE COUNT CONFIDENTIAL | CO34 |
| REPORT NUMBER 1821 | 1821 | CIRCULATION LIMITATION | |
| REPORT DATE 31 March 1964 | 0364 | CIRCULATION LIMITATION OR BIBLIOGRAPHIC | |
| [redacted] | | BIBLIOGRAPHIC (Suppl., Vol., etc.) | |

## SUBJECT ANALYSIS OF REPORT

| DESCRIPTOR | CODE | DESCRIPTOR | CODE | DESCRIPTOR | CODE |
|---|---|---|---|---|---|
| Warhead | WARH | Peak | PKNG | Kill | KILL |
| Terminal | TERI | Pressure | PRES | Mechanisms | MECH |
| Ballistics | BALS | Estimates | ESTM | Explosions | EXPS |
| Handbook | HANL | Penetration | PENE | Fragmentation | FRAG |
| Effects | EFFE | Stee' | STEE | Atmosphere | ATMO |
| Parameters | PA... | Metals | META | Weapons | WEAP |
| Fragments | FRAM | Jet | JETR | | |
| Velocity | VEL | Formation | FOR | | |
| High explosives | HIGX | Shaped | SHA | | |
| Explosives | EXPL | Charges | CHA | | |
| Blast | BLAS | Armor | ARMO | | |
| Shock waves | SHWV | Lines | LINE | | |
| Shock | SHOC | Non-nuclear | NONU | | |
| Propagation | PROO | Ordnance | ORDN | | |